Supplementary Information for

# Prolongation of singlet exciton lifetime of nonfullerene acceptor film by replacement of central benzene core with naphthalene

Tomokazu Umeyama,*[a] Kensho Igarashi,[a] Yasunari Tamai,[bc] Tatsuho Wada,[a] Taiki Takeyama,[b] Daiki Sasada,[a] Keiichi Ishida,[a] Tomoyuki Koganezawa,[d] Shunsuke Ohtani,[b] Kazuo Tanaka,[b] Hideo Ohkita*[b] and Hiroshi Imahori*[ae]

[a] Department of Molecular Engineering, Graduate School of Engineering, Kyoto University, Nishikyo-ku, Kyoto, 615-8510, Japan

[b] Department of Polymer Chemistry, Graduate School of Engineering, Kyoto University, Nishikyo-ku, Kyoto 615-8510, Japan

[c] Japan Science and Technology Agency (JST), PRESTO, 4-1-8 Honcho Kawaguchi, Saitama 332-0012, Japan

[d] Japan Synchrotron Radiation Research Institute, 1-1-1, Kouto, Sayo-cho, Sayo-gun, Hyogo 679-5198, Japan

[e] Institute for Integrated Cell-Material Sciences (WPI-iCeMS), Kyoto University, Sakyo-ku, Kyoto 606-8501, Japan

E-mail: umeyama@scl.kyoto-u.ac.jp, ohkita@photo.polym.kyoto-u.ac.jp, imahori@scl.kyoto-u.ac.jp

## Experimental

**Instruments.** $^{1}H$ NMR and $^{13}C$ NMR spectra were measured with a JEOL JNM-EX400 NMR spectrometer. High-resolution mass spectra were measured on a Thermo Fisher Scientific EXACTIVE (APCI) and LTQ orbitrp XL (MALDI). Attenuated total reflectance (ATR) FT-IR spectra were recorded on a ThermoFisher Scientific Nicolet 6700 FT-IR. Elemental analyses were performed at Organic Elemental Analysis Research Center, Kyoto University. Thermogravimetric analysis (TGA) measurements were conducted with a SHIMADZU TG-60 under flowing nitrogen at a scan rate of 10 °C $min^{-1}$. Differential scanning calorimetry (DSC) analysis was made on a SHIMADZU DSC-60 at a scan rate of 10 °C $min^{-1}$. UV–vis–near infrared (NIR) absorption spectra were obtained on a Perkin Elmer Lambda 900UV/vis/NIR spectrometer. Steady-state fluorescence spectra were recorded on a HORIBA NanoLog spectrofluorometer. Photoemission yield spectroscopy in air (PYSA) measurements were performed using an AC-3 (Riken Keiki). Time-correlated single photon counting (TCSPC) measurements using a HORIBA NanoLOG-TCSPC were conducted for fluorescence lifetime measurements on the nanosecond time-scale. The time resolution was ca. 200 ps. Absolute photoluminescence quantum efficiencies were determined using a HAMAMATSU PHOTONICS Quantaurus-QY Plus Absolute PL quantum yield spectrometer C13534-01. Atomic force microscopy (AFM) analyses were carried out with an Asylum Technology MFP-3D-SA in the AC mode.

Photocurrent–voltage characteristics were measured with Keithley 2400 SourceMeter under a nitrogen atmosphere and simulated solar light (100 mW $cm^{-2}$, AM1.5) with OTENTO-SUN III solar simulator (Bunkoukeiki). Photocurrent action spectra were recorded with CEP-2000RR (Bunkoukeiki). Current–voltage characteristics of the electron- and hole-only devices for space charge-limited current (SCLC) measurements were conducted using Keithley 2400 SourceMeter under a nitrogen atmosphere.

**Theoretical calculations.** Geometry optimization and electronic structure calculations were performed using density functional theory (DFT) at the RB3LYP/6-31G(d) level in chloroform

polarizable continuum model (PCM). Calculations were carried out using the Gaussian 09 program.[S1] All structures were fully optimized without any symmetry restriction.

**SCLC measurements.** The hole and electron mobilities were measured using the SCLC method by using devices with the configurations of ITO/PEDOT:PSS/polymer:NFA/$MoO_3$/Au for hole and ITO/ZnO/NFA/Al or ITO/ZnO/polymer:NFA/Al for electron by taking current–voltage curves and fitting the results to a space charge limited form, where the SCLC is described by:

$$J = 9\varepsilon_0\varepsilon_r\mu V^2/8L^3$$

where $\varepsilon_0$ is the permittivity of free space, $\varepsilon_r$ is the dielectric constant of the polymer, $\mu$ is the charge mobility, $V$ is the voltage drop across the device, and $L$ is the thickness of the blend film. The dielectric constant $\varepsilon_r$ is assumed to be 3, which is a typical value for organic semiconductors.

**GIWAXS measurements.** Samples were prepared by spin-coating the NFA, polymer, or polymer:NFA solution on the ITO/ZnO substrate as conducted in the OPV device fabrications. GIWAXS measurements were conducted at the SPring-8 on beamline BL46XU. The sample was irradiated at a fixed incident angle on the order of 0.12 ° through a Huber diffractometer with X-ray energy of 12.398 keV (X-ray wavelength $\lambda$ = 0.10002 nm), and the GIWAXS patterns were recorded with a 2D image detector (Pilatus 300 K) with the sample-to-detector distances of 173.8 mm.

**OPV device fabrication.** OPV devices were prepared on patterned indium tin oxide (ITO) substrates which were cleaned by ultra-sonication in deionized water, $CHCl_3$, acetone, and tetramethyl-ammonium hydroxide aqueous solution for 15 min each, and then deionized water for 25 min, followed by 2-propanol and ethanol for 15 min each. They were subsequently dried under nitrogen flow, and treated in a UV–ozone cleaner for 25 min. A solution of $Zn(OAc)_2{\cdot}2H_2O$ (33 mg), 2-methoxyethanol (1 mL), ethanolamine (9.4 μL) stirred at room temperature, and was spin-coated on substrates at 3000 rpm for 20 s. The ZnO layer was dried at 200 °C for 30 min, and then transferred into a glove box filled with dried $N_2$ gas to coat the active layer.

A photoactive layer of PBDB-T:NTTIC was fabricated according to the following procedure. A blend solution of PBDB-T and NTTIC with a polymer concentration of 10 mg $mL^{-1}$ (1:1 ratio by weight) in chlorobenzene with 1,8-diidooctane (0.5 vol.%) was prepared and stirred on a hotplate at 25 °C 400 rpm for 3 h. The active layer was spin-coated at 1750 rpm for 20 s on the top of the ZnO layer, and the samples were annealed at 160 °C for 10 min. The thickness of the photoactive layer was ca. 100 nm.

A photoactive layer of PBDB-T:ITIC was fabricated according to the following procedure. A blend solution of PBDB-T with ITIC ([PBDB-T] = 9 mg $mL^{-1}$, [PBDB-T]:[ITIC] = 1:0.7, w/w) in chlorobenzene with 1,8-diiodooctane (0.5 vol.%) was prepared and stirred on a hotplate at 40 °C for 3 h. The active layer was spin-coated at 2000 rpm for 20 s on the top of the ZnO layer, and the samples were annealed at 100 °C for 10 min. The thickness of the photoactive layer was ca. 100 nm.

All samples were finally transferred to an evaporation chamber for $MoO_3$ deposition (~10 nm) at a rate of 0.1–0.3 Å $s^{-1}$ and Ag deposition (~100 nm) at a rate of 1–2 Å $s^{-1}$ before extracting their *J*–*V* characteristics (under AM1.5 conditions).

**Femtosecond transient absorption.** Femtosecond transient absorption data were collected with a pump and probe femtosecond transient spectroscopy system. This system consists of a regenerative amplified Ti:sapphire laser (Spectra-Physics, Hurricane) and a transient absorption spectrometer (Ultrafast systems, Helios). The amplified Ti:sapphire laser provided 800 nm fundamental pulses at a repetition rate of 1 kHz with an energy of 0.8 mJ and a pulse width of 100 fs (full-width at half-maximum), which were split into two optical beams with a beam splitter to generate pump and probe pulses. One fundamental beam was converted into white-light pulses employed as probe pulses in the wavelength region from 450 to 1300 nm. The other fundamental beam was used as pump pulses at 700 nm after conversion with an ultrafast optical parametric amplifier (Spectra-Physics, TOPAS). The pump pulses were modulated mechanically at a repetition rate of 500 Hz. Temporal evolution of the probe intensity was recorded with a CMOS linear sensor (Ultrafast Systems, SPEC-VIS) for visible measurements, and with an InGaAs linear diode array sensor (Ultrafast Systems, SPEC-NIR) for NIR

measurements. Transient absorption spectra and decays were collected over the time range of −5 ps to 3 ns. Typically, 2500 laser shots were averaged at each delay time to obtain a detectable absorbance change as small as ~$10^{-4}$. To cancel out orientation effects on the dynamics, the polarization direction of the linearly polarized probe pulse was set at the magic angle of 54.7 ° with respect to that of the pump pulse. The sample films were encapsulated in a $N_2$ filled glove box. Note that the transient absorption spectra and dynamics were highly reproducible even after several measurements. In other words, the laser irradiation had negligible effects on the sample degradation at least under those experimental conditions.

## Synthetic Procedures

**Materials.** Ethyl 2-bromothieno[3,2-*b*]thiophene-3-carboxylate,[S2] 2,6-bis(4,4,5,5-tetramethyl-1,3,2-dioxaborolan-2-yl)naphthalene,[S3] 2-(3-oxo-2,3-dihydro-1*H*-inden-1-ylidene)malononitrile (IC),[S4] and tetrakis(triphenylphosphine)palladium(0) ($Pd(PPh_3)_4$)[S5] were synthesized according to the reported procedures. PBDB-T, J71, and ITIC were purchased from 1-Material. All other chemicals were purchased from commercial supplier and used without further purification.

**Synthesis.**

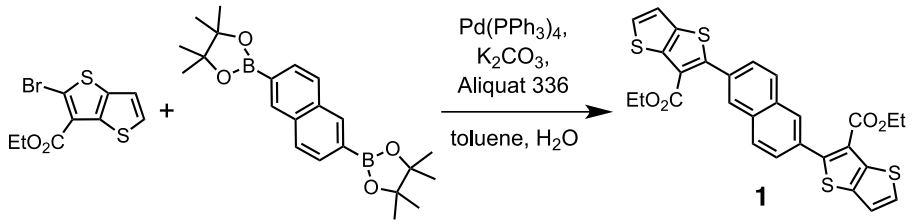


**Compound 1.** A solution of ethyl 2-bromothieno[3,2-*b*]thiophene-3-carboxylate (597 mg, 2.05 mmol, 2.4 equiv.), 2,6-bis(4,4,5,5-tetramethyl-1,3,2-dioxaborolan-2-yl)naphthalene (326 mg, 0.858 mmol, 1 equiv.), and small amount of Aliquat 336 in toluene (9 mL) and $K_2CO_3$ aq. (2M, 2.8 mL) was deoxygenated with Ar for 30 min, and then $Pd(PPh_3)_4$ (99.6 mg, 0.0862 mmol, 0.10 equiv.) was added to the mixture. After the reaction mixture was stirred overnight at 100 °C, the reaction was

filtrated and the residue was washed with a small amount of chloroform. The crude product of compound **1** was obtained as a pale yellow solid and used in the next step without further purification.

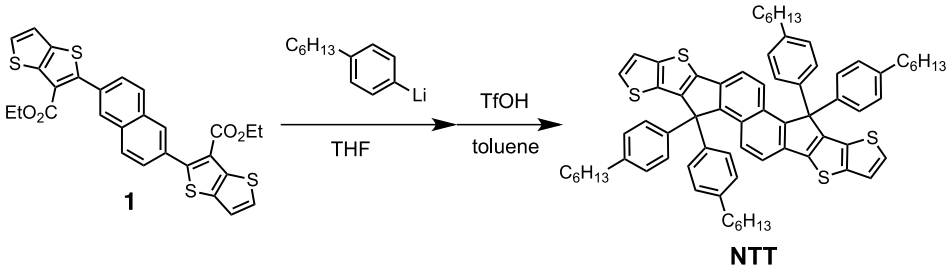


**NTT.** To a solution of 4-hexyl-1-bromobenzene (1.74 mL, 8.52 mmol, 10 equiv.) in THF (17 mL) at –78 °C, *n*-BuLi (1.57 M, 5.40 mL, 8.48 mmol, 10 equiv.) was added under an Ar atmosphere, and then the mixture was stirred at –78 °C for 1 h. A solution of crude product of compound **1** (less than 0.858 mmol, 1 equiv.) in THF (100 mL) was added slowly. After the addition, the mixture was gradually warmed up to room temperature and then stirred at reflux for 2 h. The reaction was quenched with water, extracted with $CHCl_3$, and combined organic phase was dried over $Na_2SO_4$. After filtration, the solvent was removed under reduced pressure. The crude product was obtained and used in the next step without further purification. To a solution of the crude product in toluene (50 mL), 3 drops of trifluoromethanesulfonic acid (TfOH) were added before stirred at 70 °C for 1 h. The reaction was quenched with water, extracted with $CHCl_3$, and combined organic phase was dried over $Na_2SO_4$. After filtration, the solvent was removed under reduced pressure, and the resulting residue was purified by column chromatography with hexane/$CHCl_3$ = 1:0 to 4:1 as eluent. NTT was obtained as a yellow solid (310 mg, yield: 33.9% in 3 steps). The purity of the target compound was >99.9% according to the peak area ratios in the $^1$H NMR spectrum. $^1$H NMR (400 MHz, $CDCl_3$, ppm): δ 7.90 (d, $J$ = 8.4 Hz, 2H), 7.50 (d, $J$ = 8.0 Hz, 2H), 7.25–7.20 (m, 12H), 7.05 (d, $J$ = 8.4 Hz, 8H), 2.53 (t, $J$ = 8.0 Hz, 8H), 1.59–1.52 (m, 4H), 1.32–1.23 (m, 28H), 0.85 (t, $J$ = 6.8Hz, 12H). $^{13}$C NMR (100 MHz, $CDCl_3$, ppm): δ 149.69, 149.32, 143.06, 141.75, 137.65, 134.94, 133.38, 129.07, 129.01, 128.44, 126.42, 125.97, 120.46, 118.79, 64.47, 36.70, 31.82, 31.28, 29.30, 22.72, 14.22. HRMS (p MALDI) calcd for $[C_{72}H_{76}S_4]^+$: 1068.4824; found: 1068.4796. IR (ATR, cm$^{-1}$): $\nu_{max}$ 2959, 2925, 2853, 1504, 1451, 1370, 1333, 1184, 1079, 1020, 874, 816, 702, 664, 636, 588, 567. Melting point: 110–111 °C.

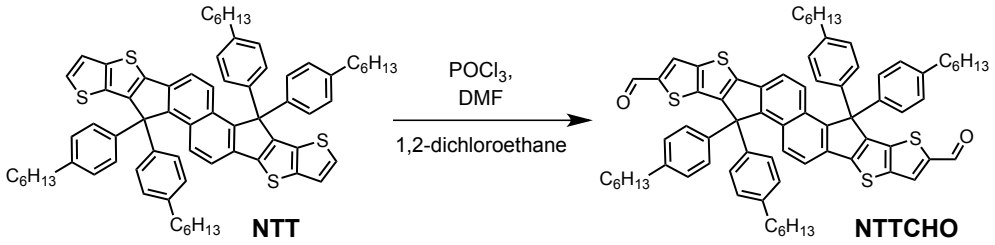


**NTTCHO.** Vilsmeier reagent was prepared according to the following procedure. $POCl_3$ (1 mL, 10.7 mmol, 58 equiv.) was added to DMF (8 mL) at 0 °C and stirred at 0 °C for 1 h under an Ar atmosphere. To a solution of NTT (199.4 mg, 0.186 mmol, 1 equiv.) in 1,2-dichloroethane (16 mL), the Vilsmeier reagent was added at 0 °C. The mixture was stirred at room temperature for 2 h and then at 80 °C for 2 h. After cooling down to room temperature, the reaction was quenched with AcONa aq., extracted with $CHCl_3$, and the organic phase was dried over $Na_2SO_4$. After filtration, the solvent was removed under reduced pressure, and the resulting residue was purified by column chromatography with hexane/$CHCl_3$ = 1:2 as eluent to give a solid, which was further purified by reprecipitation with $CHCl_3$/ethanol. NTTCHO was obtained as an orange solid (199.1 mg, yield: 94.9%). The purity of the target compound was >99.9% according to the peak area ratios in the $^1$H NMR spectrum. $^1$H NMR (400 MHz, $CDCl_3$, ppm): δ 9.86 (s, 2H), 7.97 (d, $J$ = 8.4 Hz, 2H), 7.91 (s, 2H), 7.57 (d, $J$ = 8.8 Hz, 2H), 7.21 (d, $J$ = 8.0 Hz, 8H), 7.07 (d, $J$ = 8.8 Hz, 8H), 2.53 (t, $J$ = 7.8 Hz, 8H), 1.59–1.52 (m, 4H), 1.34–1.23 (m, 28H), 0.85 (t, $J$ = 6.8Hz, 12H). $^{13}$C NMR (100 MHz, $CDCl_3$, ppm): δ 183.02, 151.05, 149.87, 149.64, 143.83, 142.34, 141.71, 139.82, 136.56, 134.71, 130.05, 128.82, 128.73, 127.11, 119.43, 64.59, 35.69, 31.81, 31.29, 29.29, 22.70, 14.22. HRMS (p MALDI) calcd for $[C_{74}H_{76}O_2S_4+H]^+$: 1125.4723; found: 1125.4764. IR (ATR, $cm^{-1}$): $\nu_{max}$ 2923, 2853, 1655, 1492, 1459, 1433, 1370, 1284, 1222, 1186, 1128, 1091, 1019, 818, 670, 649. Melting point: >300 °C.

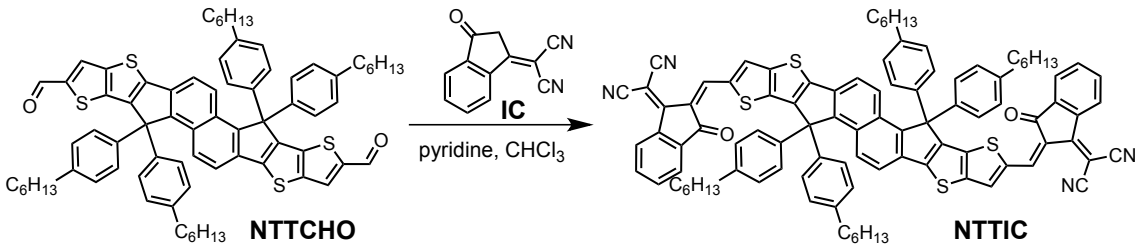

**NTTIC.** A solution of NTTCHO (156 mg, 0.138 mmol, 1 equiv.) and 2-(3-oxo-2,3-dihydro-1*H*-inden-1-ylidene)malononitrile (IC, 133 mg, 0.685 mmol, 4.9 equiv.) in $CHCl_3$ (35 mL) was deoxygenated with Ar for 30 min. After 4 drops of pyridine were added, the reaction was stirred at reflux for 2 days. The crude product was reprecipitated with $CHCl_3$/EtOH, and the resulting residue was purified by column chromatography with hexane/$CHCl_3$ = 1:2 as eluent, reprecipitated with $CHCl_3$/EtOH again. NTTIC was obtained as a dark blue solid (196 mg, yield: 95.6%). The purity of the target compound was >99.9% according to the peak area ratios in the $^1$H NMR spectrum. $^1$H NMR (400 MHz, $CDCl_3$, ppm): δ 8.83 (s, 2H), 8.67 (d, $J$ = 6.4 Hz, 2H), 8.19 (s, 2H), 8.03 (d, $J$ = 8.8 Hz, 2H), 7.92 (m, 2H), 7.78–7.72 (m, 4H), 7.56 (d, $J$ = 8.8 Hz, 2H), 7.29 (d, $J$ = 8.4 Hz, 8H), 7.12 (d, $J$ = 8.0 Hz, 8H), 2.54 (t, $J$ = 8.0 Hz, 8H), 1.34–1.23 (m, 32H), 0.83 (t, $J$ = 6.8 Hz, 12H). $^{13}$C NMR (100 MHz, $CDCl_3$, ppm): δ 188.28, 160.45, 153.25, 152.23, 150.55, 146.81, 143.55, 142.52, 140.10, 139.00, 138.41, 137.17, 136.95, 136.30, 135.23, 134.89, 134.57, 129.89, 128.90, 127.58, 125.37, 123.82, 122.45, 119.69, 114.82, 114.73, 69.23, 64.75, 35.70, 31.81, 31.27, 29.84, 29.30, 22.70, 14.20. HRMS (p MALDI) calcd for $[C_{98}H_{84}N_4O_2S_4]^+$: 1476.5472; found: 1476.5444. IR (ATR, $cm^{-1}$): $\nu_{max}$ 2922, 2852, 2217, 1700, 1537, 1466, 1452, 1391,1339, 1305, 1281, 1243, 1154, 1128, 1020, 991, 912, 817, 771, 719. Melting point: >300 °C. Anal. Calcd for $C_{98}H_{84}N_4O_2S_4$: C, 79.64; H, 5.73; N, 3.79; O, 2.17; S, 8.68. Found: C, 78.81; H, 5.79; N, 3.53; O, 2.18; S, 8.65.

## Supporting Notes

**Signal assignments in transient absorption spectrum of PBDB-T:NTTIC.** Fig. 4 shows the transient absorption spectrum of the PBDB-T:NTTIC blend film measured at 0–2500 ps. Immediately after the photoexcitation at 700 nm, at which NTTIC was preferentially excited (Fig. S13), an absorption band with a peak at 1000 nm was observed, which can be assigned to the absorption of the $S_1$ state of NTTIC (Fig. S11). In addition, a negative peak appeared at 700 nm due to the ground state bleaching (GSB) of NTTIC (Fig. S13a). A negative shoulder signal also emerged at 570 nm assignable to the GSB of PBDB-T (Fig. S13a). A negative peak at 630 nm can be attributed to the sum of GSBs of NTTIC and PBDB-T (Fig. S13a).

The transient absorption spectrum of PBDB-T:NTTIC at 2500 ps exhibited a broad absorption band in 700–1000 nm region with peaks at 720 and 920 nm (Fig. 4), although the $S_1$ signal of NTTIC at 1000 nm already disappeared. To explore the origin of these absorption bands, first we observed the changes in the absorption spectrum of NTTIC by chemical reduction with cobaltocene (Fig. S14a–c). When adding an equivalent amount of cobaltocene to NTTIC solution in benzonitrile, the differential absorption spectrum showed an intense negative peak at 658 nm and a positive peak at 745 nm (Fig. S14b,c). Then, we also implemented the chemical oxidation of PBDB-T using magic blue (tris(4-bromophenyl)ammoniumyl hexachloroantimonate) as an oxidant and observed the changes in the absorption spectrum of PBDB-T (Fig. S14d,e). When adding $9.5 \times 10^{-9}$ mol of magic blue in $CH_2Cl_2$ (10 μL) to PBDB-T ($4.2 \times 10^{-8}$ mol by repeating unit) in $CHCl_3$ (3 mL), the differential absorption spectrum showed negative peaks at 580 and 630 nm and positive peaks at 700 and 930 nm (Fig. S14d,e). Considering these results, we assigned the absorption bands in the transient absorption spectrum of PBDB-T:NTTIC at 2500 ps to both the NTTIC radical anion and the PBDB-T hole polaron.[S6–S8] These assignments suggested the occurrences of the charge transfer (CT) and charge dissociation (CD) by the photoexcitation.

**Decay dynamics of $S_1$ of NTTIC and charge-separated states in PBDB-T:NTTIC with various excitation intensities.** Although the $S_1$ of NTTIC showed a relatively strong absorption band at 1000 nm in the transient absorption spectrum of PBDB-T:NTTIC (Fig. 4), the substantial overlapping with the band of the PBDB-T hole polaron complicated the estimation of the $S_1$ lifetime of NTTIC by monitoring the transient absorption intensity at 1000 nm. Instead, we monitored GSB of PBDB-T at 570 nm with the excitation intensities of 2.1–15.8 μJ $cm^{-2}$. Fig. S15a displays the time profiles at 0–100 ps. Because the excitation light of 700 nm was preferentially absorbed by NTTIC in the PBDB-T:NTTIC blend film, the growth of the PBDB-T GSB at 570 nm originated from the interaction of PBDB-T with the excited ITIC, i.e., CT. After the photoexcitation at the intensity of 2.1 μJ $cm^{-2}$, the GSB signal of PBDB-T grew with the time constant of ca. 14 ps (Fig. S15a), indicating that $S_1$ of NTTIC decayed with this time constant. The lowest pump fluence was empolyed for the estimation

of the time constant to minimize the effects of multiphoton absorptions or bimolecular deactivation processes between excitons and/or charges. At the excitation intensity of 15.8 μJ $cm^{-2}$, the GSB signal of PBDB-T clearly showed a decay at >20 ps, suggesting the occurrence of bimolecular deactivation processes of PBDB-T hole polaron such as nongeminate recombination due to the relatively strong excitation intensity.

Fig. S15b depicts the TA time profiles of PBDB-T:NTTIC at 570 nm with the excitation intensities of 2.1–15.8 μJ $cm^{-2}$. This corresponds to the GSB recovery profiles of PBDB-T. The dynamics was independent of the excitation intensity of ≤7.5 μJ $cm^{-2}$, suggesting that the bimolecular deactivation processes for the charges were absent in this time scale. Therefore, we estimated the CD efficiency to be 0.76 from the TA recovery profiles at 570 nm with the excitation energy of ≤7.5 μJ $cm^{-2}$. In addition, the CD efficiency could also be estimated from TA time profiles at 730 nm, in which both the PBDB-T hole polaron and the NTTIC radical anion possess absorption, with the excitation energy of ≤7.5 μJ $cm^{-2}$ (Fig. S15c), resulting in the consistent value (0.76).

**Table S1** Absorption and PL maxima ($\lambda_{abs}$ and $\lambda_{PL}$)[a] and optical gap energies ($E_{g,opt}$)[b] of NTTIC and ITIC in solution and film states.

| NFA | $\lambda_{abs,sol}$ / nm | $\lambda_{PL,sol}$ / nm | $E_{g,opt,sol}$ / eV | $\lambda_{abs,film}$ / nm | $\lambda_{PL,film}$ / nm | $E_{g,opt,film}$ / eV |
|---|---|---|---|---|---|---|
| NTTIC | 672 | 713 | 1.79 | 692 | 745 | 1.72 |
| ITIC | 678 | 716 | 1.78 | 711 | 760 | 1.68 |

[a] Chloroform was used as a solvent for solution. [b] Determined by the energies at the intersection points of normalized absorption and PL spectra.

**Table S2** HOMO/LUMO energy levels and electron mobilities ($\mu_e$)[a] of NTTIC and ITIC.

| NFA | HOMO[b] / eV | LUMO[c] / eV | HOMO[d] / eV | LUMO[d] / eV | $\mu_e$ / $10^{-4}$ $cm^2$ $V^{-1}$ $s^{-1}$ |
|---|---|---|---|---|---|
| NTTIC | −5.68 | −3.96 | −5.46 | −3.39 | 4.6 |
| ITIC | −5.71 | −4.03 | −5.52 | −3.46 | 2.6 |

[a] Measured by SCLC with the device configuration of ITO/ZnO/NFA/Al. [b] Determined by PYSA. [c] Determined by HOMO + optical bandgap in the film states. [d] Calculated from DFT.

**Table S3** Singlet exciton lifetime ($^{\tau_{S_1}}$),[a] PL quantum yield ($\Phi_{PL}$),[b] radiative rate constant ($k_r$),[c] and nonradiative rate constant ($k_{nr}$)[c] of NTTIC in chloroform solution and film.

| sample | $^{\tau_{S_1}}$ / ps | $\Phi_{PL}$ | $k_r$ / $s^{-1}$ | $k_{nr}$ / $s^{-1}$ |
|---|---|---|---|---|
| NTTIC solution | 210[c] | 0.049 | $2.3 \times 10^8$ | $4.6 \times 10^9$ |
| NTTIC film | 280[c] | 0.029 | $1.0 \times 10^8$ | $3.5 \times 10^9$ |

[a] Estimated by the PL decay. [b] Estimated by the integrated sphere method. [c] $k_r$ and $k_{nr}$ are calculated from the experimental data of $\Phi_{PL}$ and $^{\tau_{S_1}}$, according to the following equations; $\Phi_{PL} = k_r \times (k_r + k_{nr})^{-1}$ and $^{\tau_{S_1}} = (k_r + k_{nr})^{-1}$.

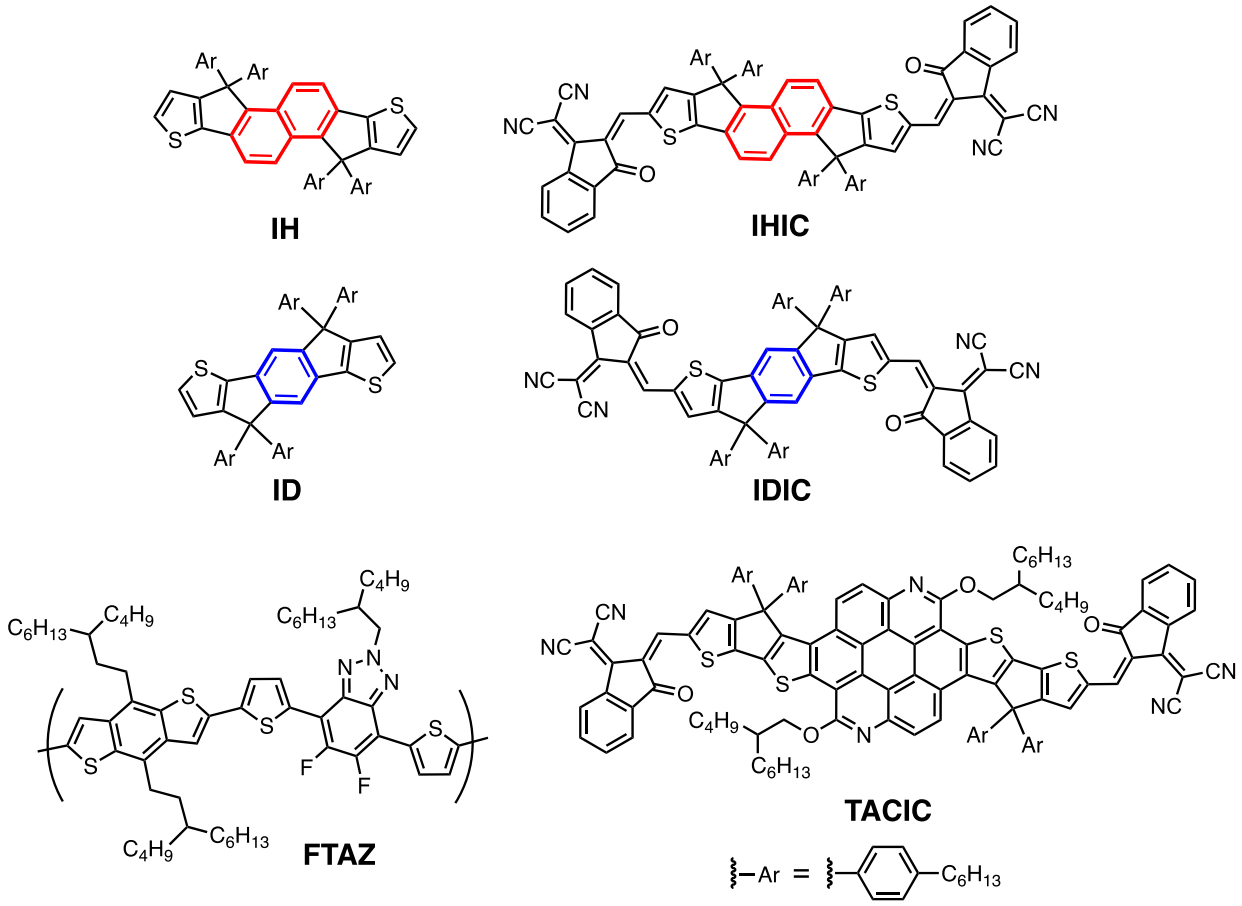


**Fig. S1** Chemical structures of IH, IHIC, ID, IDIC, FTAZ, and TACIC.

(a)

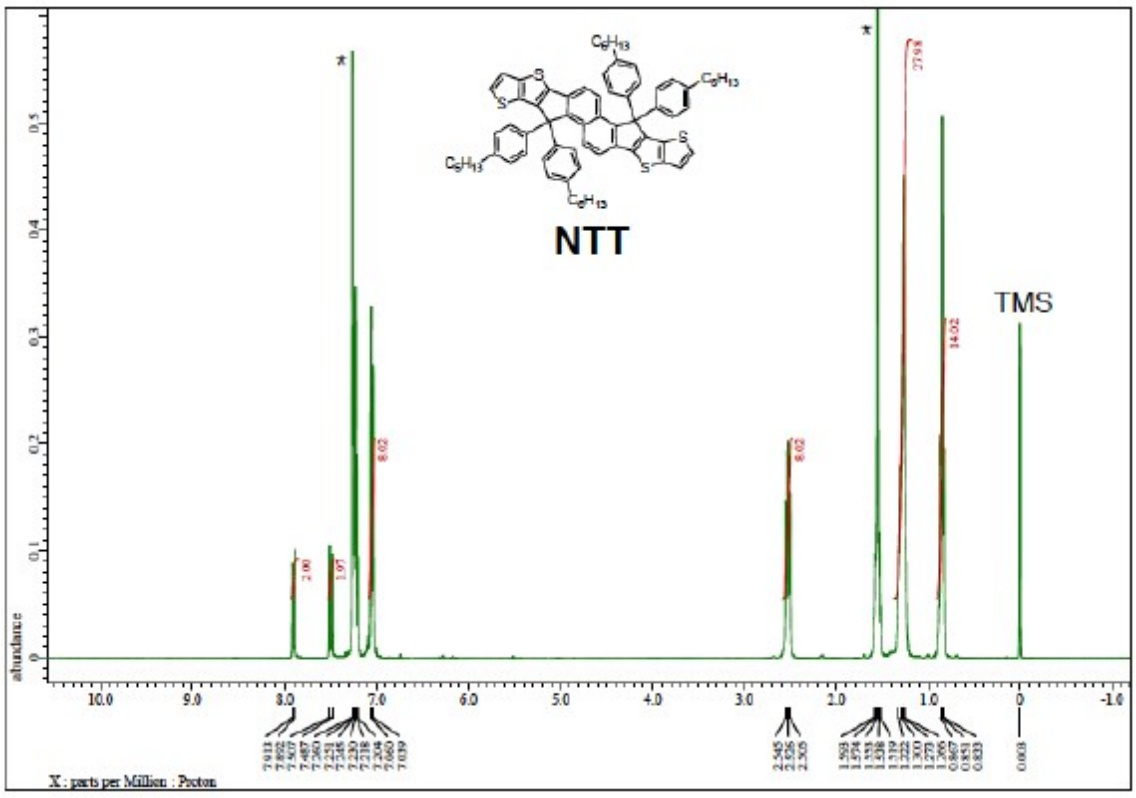
NTT
TMS
abundance
X : parts per Million : Proton

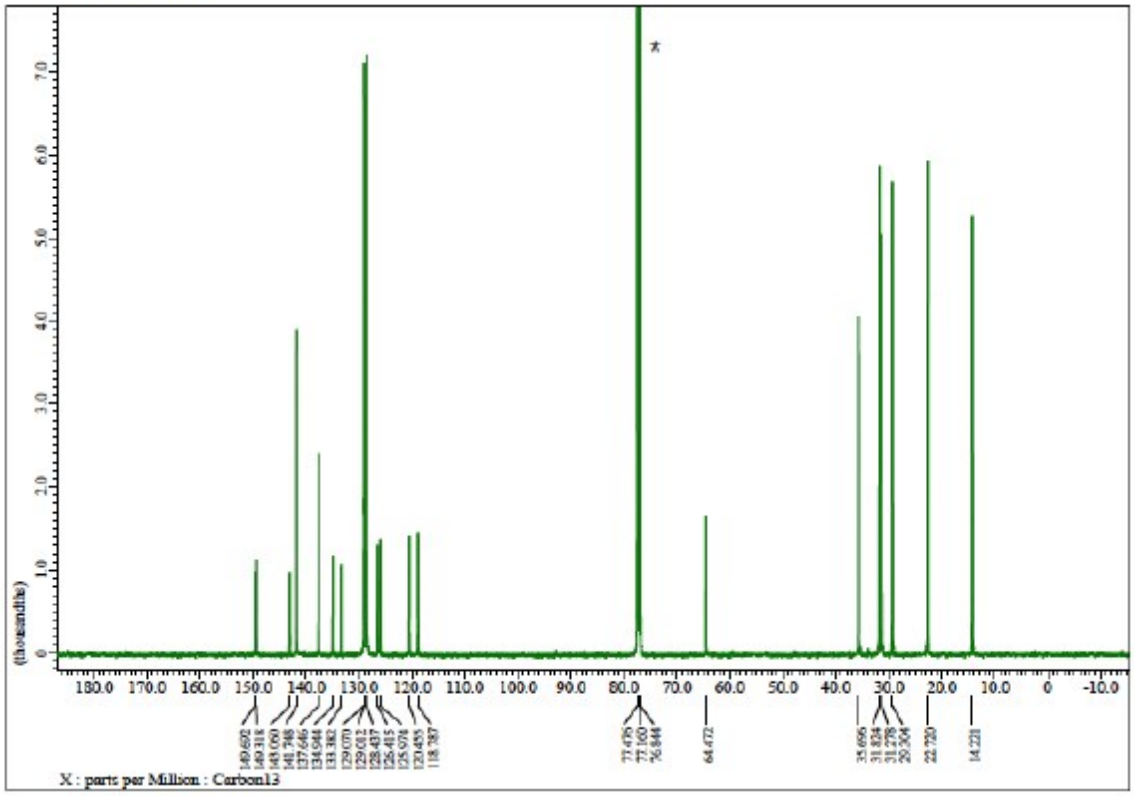
(thousands)
X : parts per Million : Carbon13

(b)

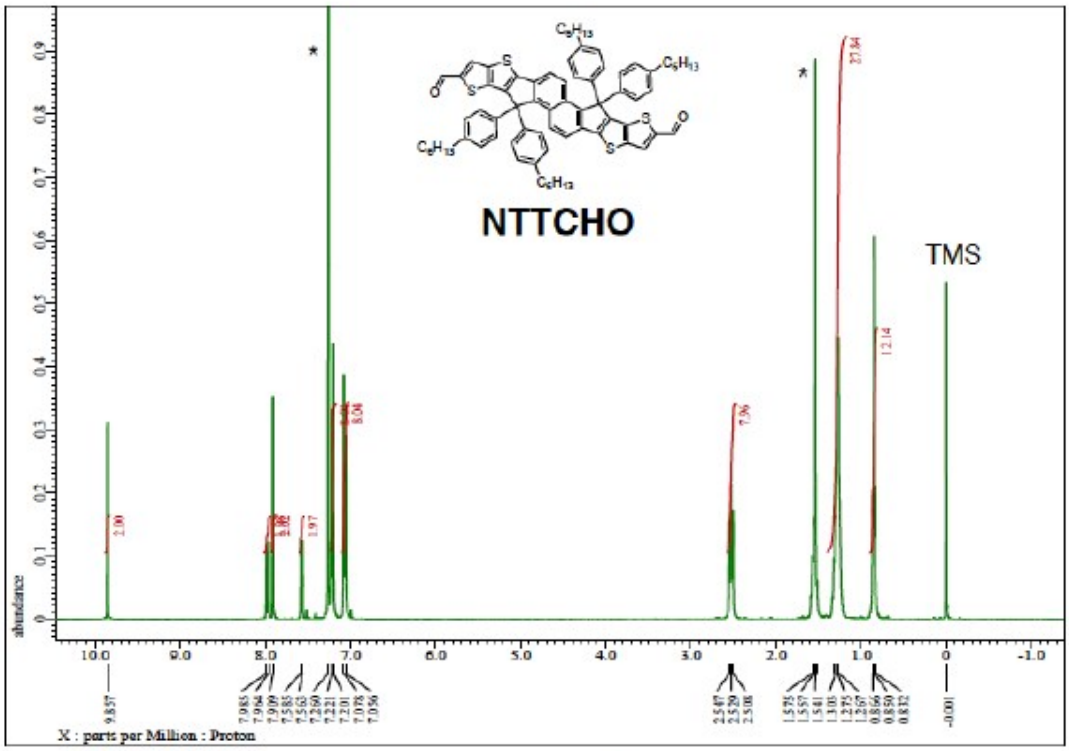
NTTCHO
TMS
abundance
X : parts per Million : Proton

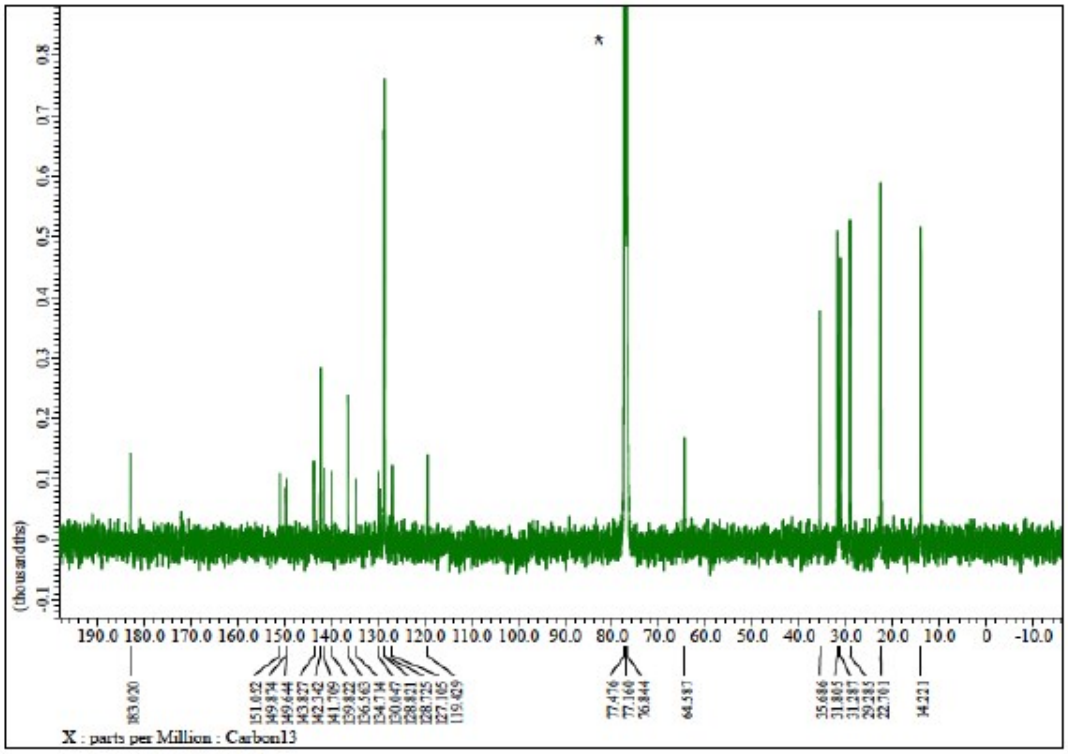
(thousandths)
X : parts per Million : Carbon13

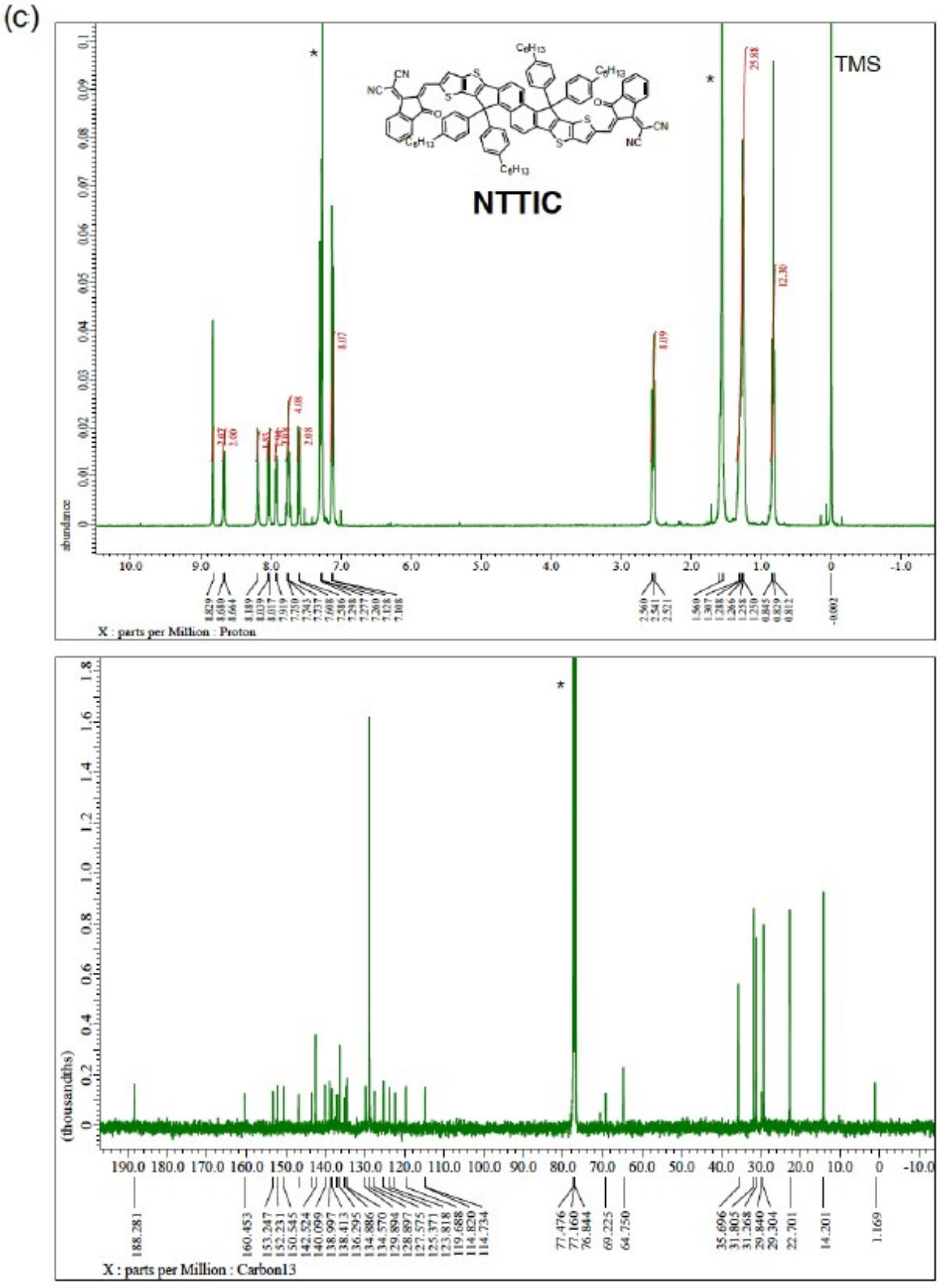


**Fig. S2** $^{1}H$ (upper) and $^{13}C$ (lower) NMR spectra of (a) NTT, (b) NTTCHO, and (c) NTTIC in $CDCl_3$. Peaks marked with * arise from residual solvents.

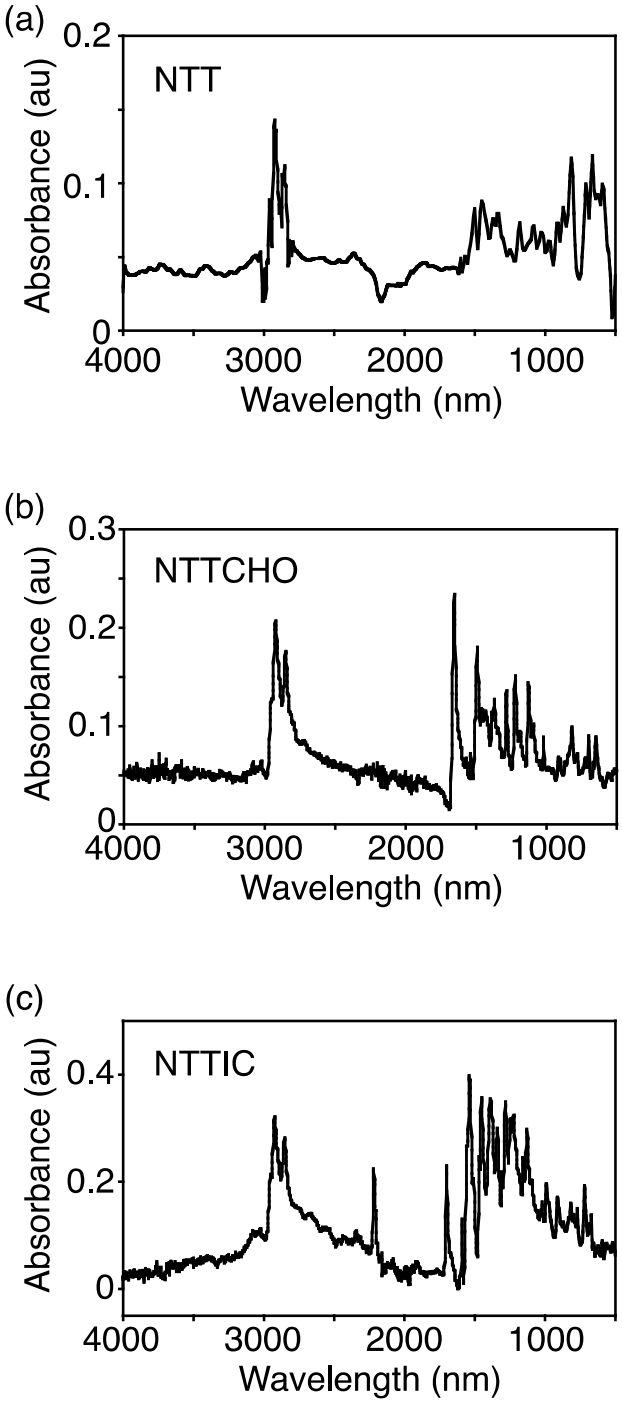


**Fig. S3** ATR FT-IR spectra of (a) NTT, (b) NTTCHO, and (c) NTTIC.

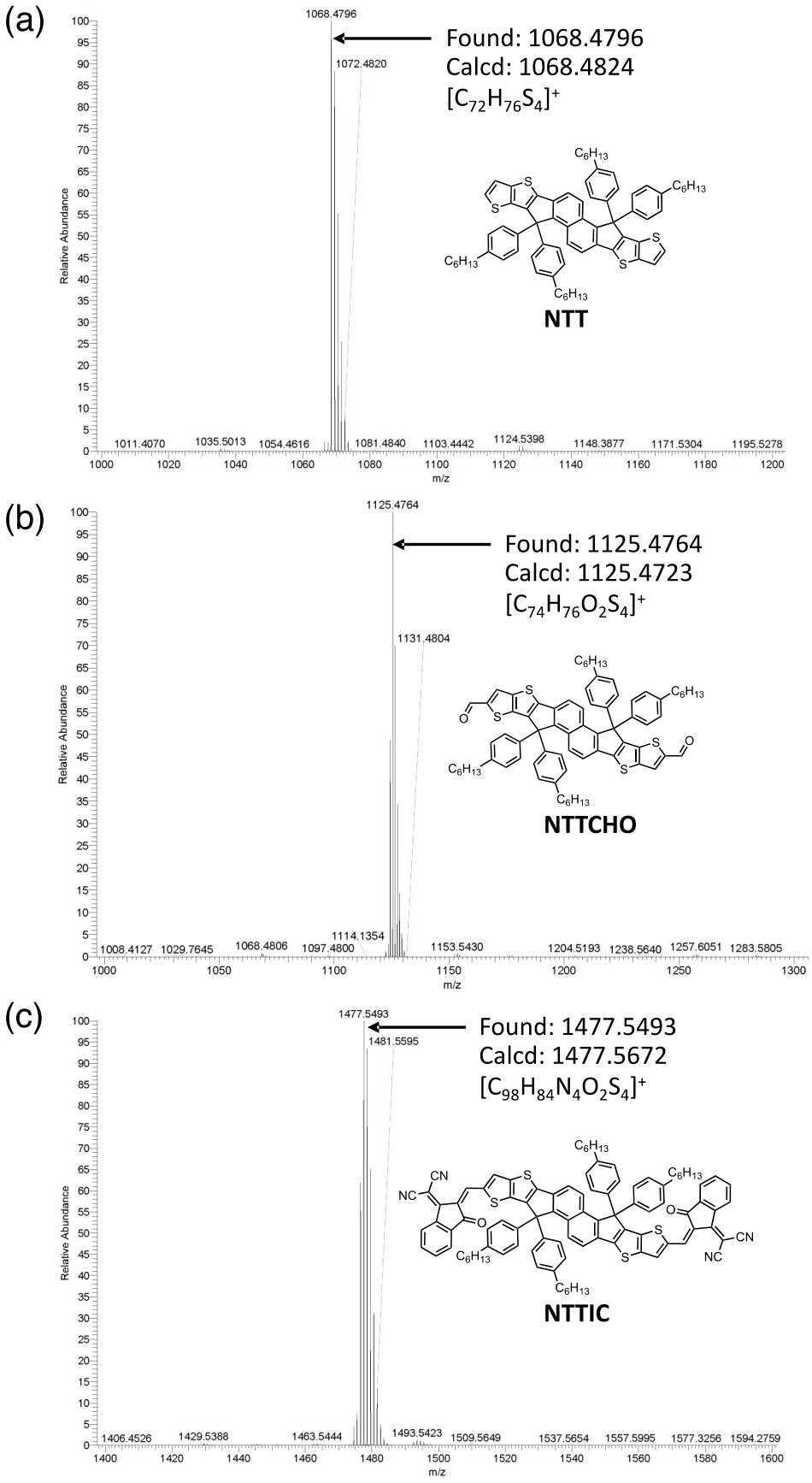


**Fig. S4** High-resolution mass spectra of (a) NTT, (b) NTTCHO, and (c) NTTIC.

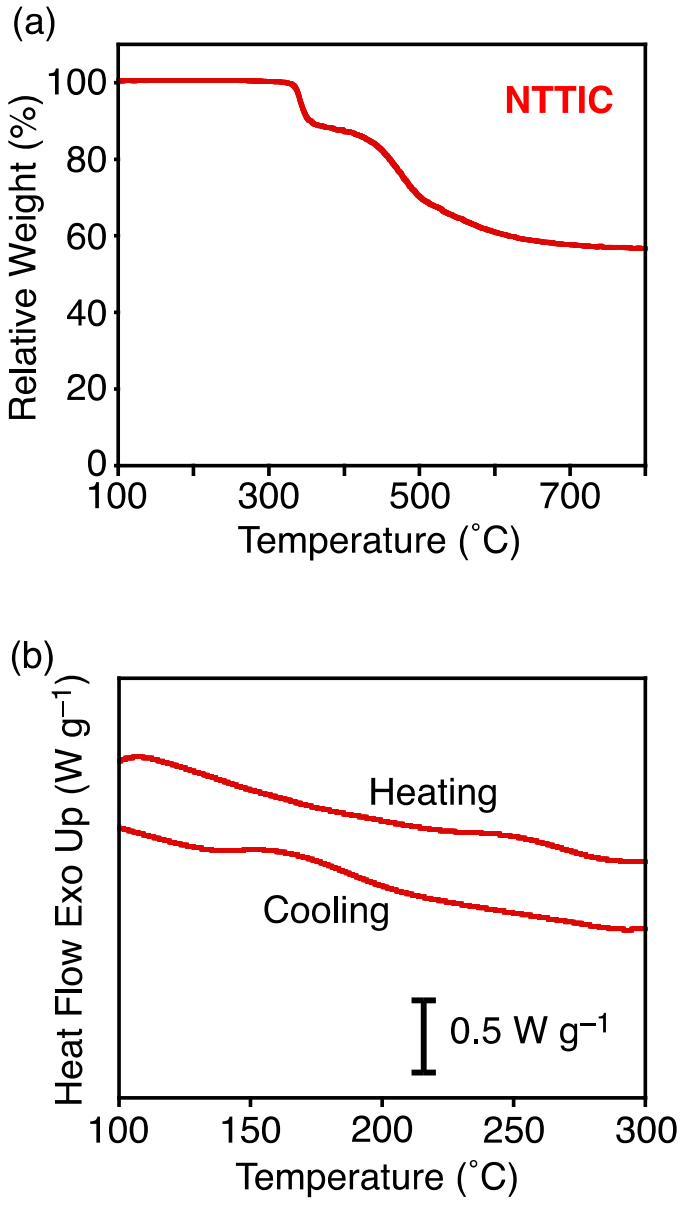


**Fig. S5** (a) TGA and (b) DSC curves of NTTIC. The analyses were performed under flowing nitrogen at a scan rate of 10 °C $min^{-1}$. The decomposition temperature ($T_d$, 5% weight loss) was estimated to be 345 °C in (a).

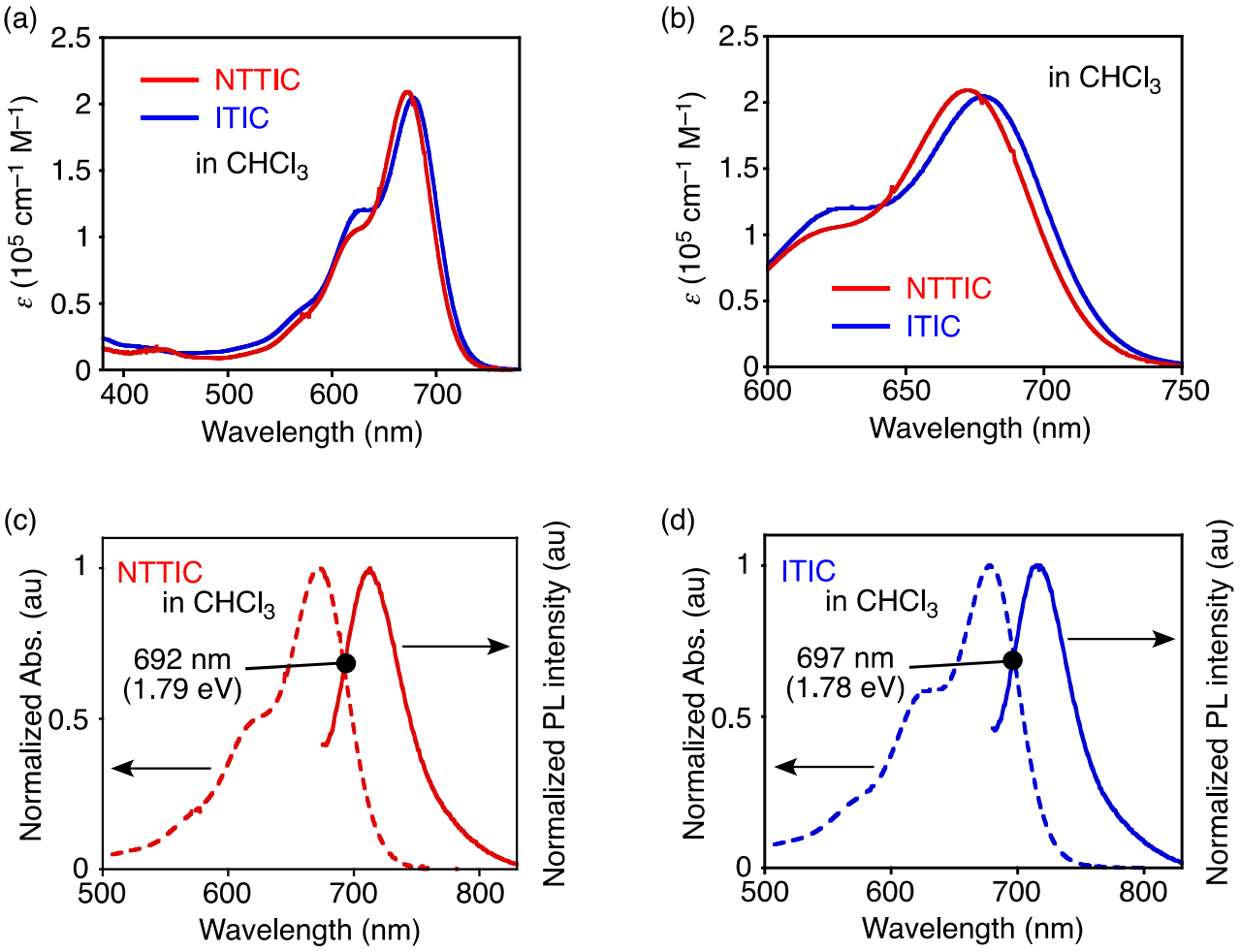


**Fig. S6** (a) UV–vis–NIR absorption spectra of NTTIC and ITIC in chloroform. (b) Enlarged image of (a) around the absorption peak positions. (c,d) Normalized UV–vis–NIR absorption and fluorescence spectra of (b) NTTIC and (c) ITIC in chloroform. The excitation wavelengths for fluorescence measurements are the absorption maxima. The wavelengths and energies at the intersection points are shown in the figures.

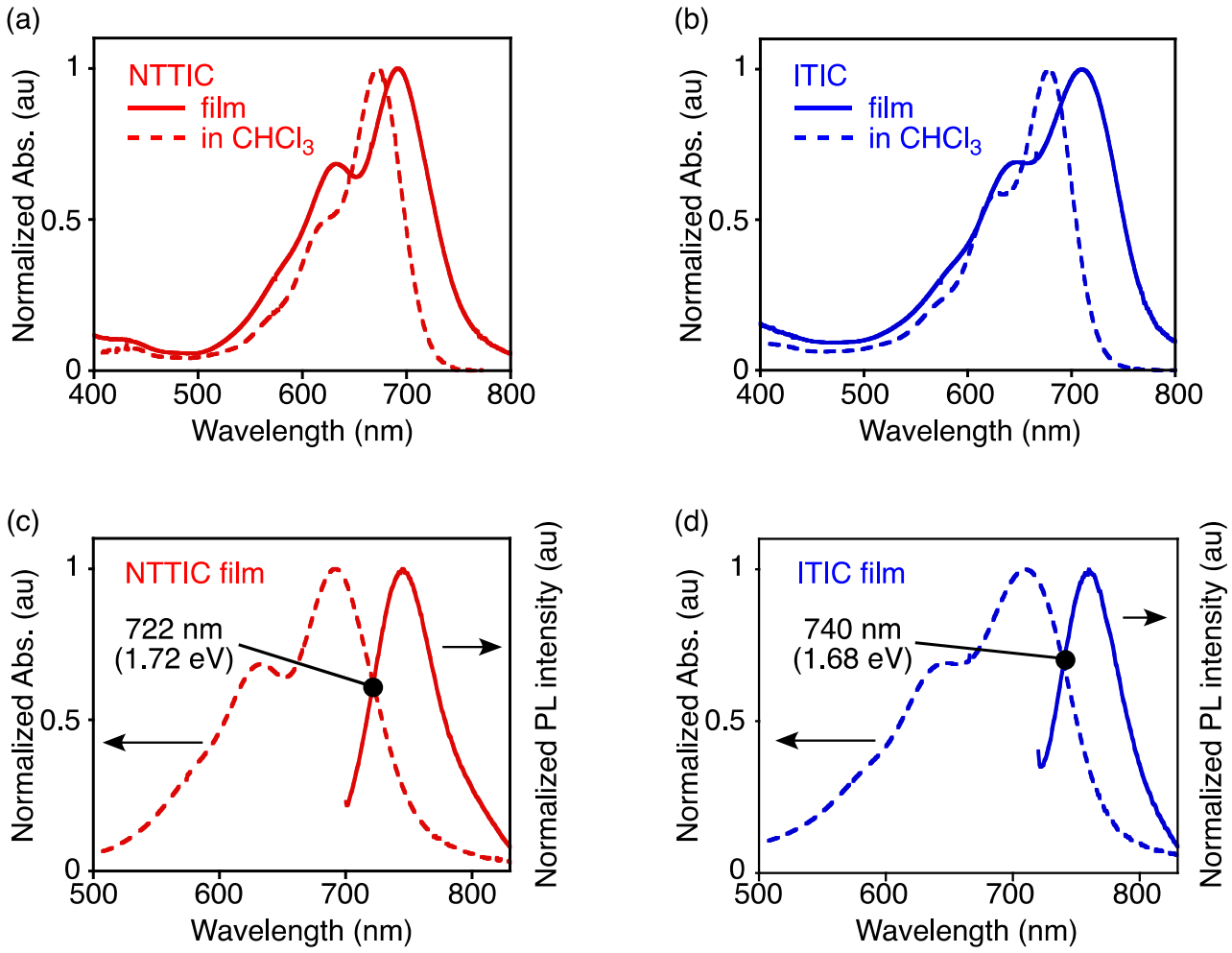


**Fig. S7** (a,b) Normalized UV–vis–NIR absorption spectra of (a) NTTIC and (b) ITIC chloroform solutions and films. (c,d) Normalized UV–vis–NIR absorption and fluorescence spectra of (c) NTTIC and (d) ITIC films. The excitation wavelengths for fluorescence measurements are the absorption maxima. The wavelengths and energies at the intersection points are shown in (c) and (d).

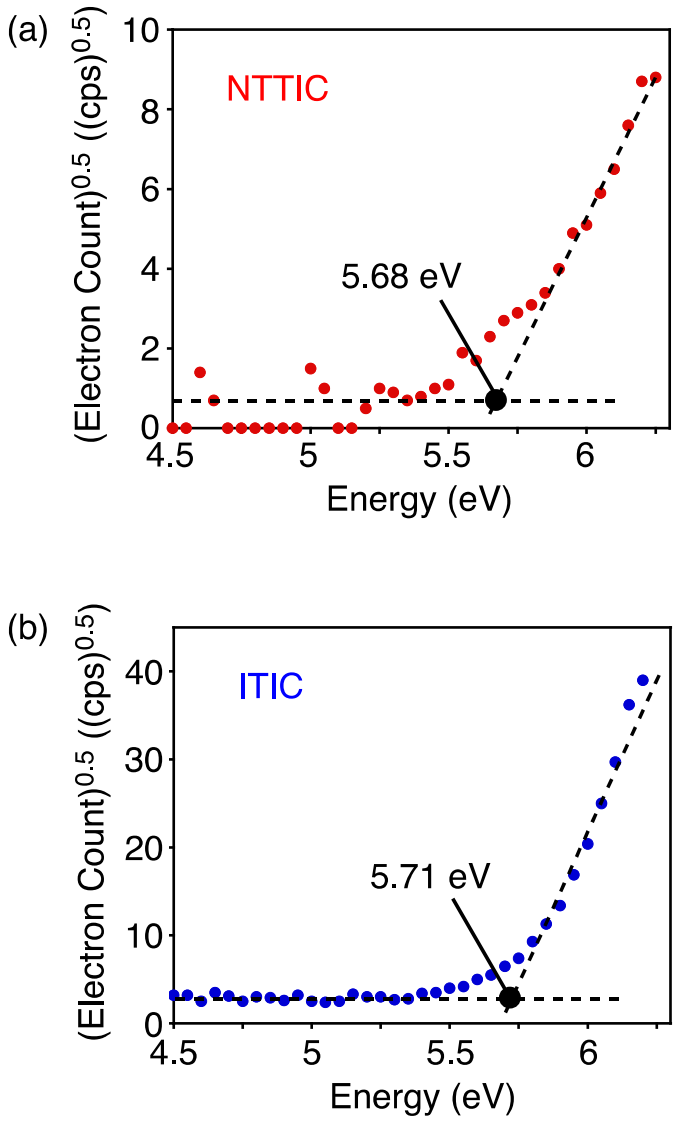


**Fig. S8** Photoemission yield spectroscopy in air (PYSA) of (a) NTTIC and (b) ITIC.

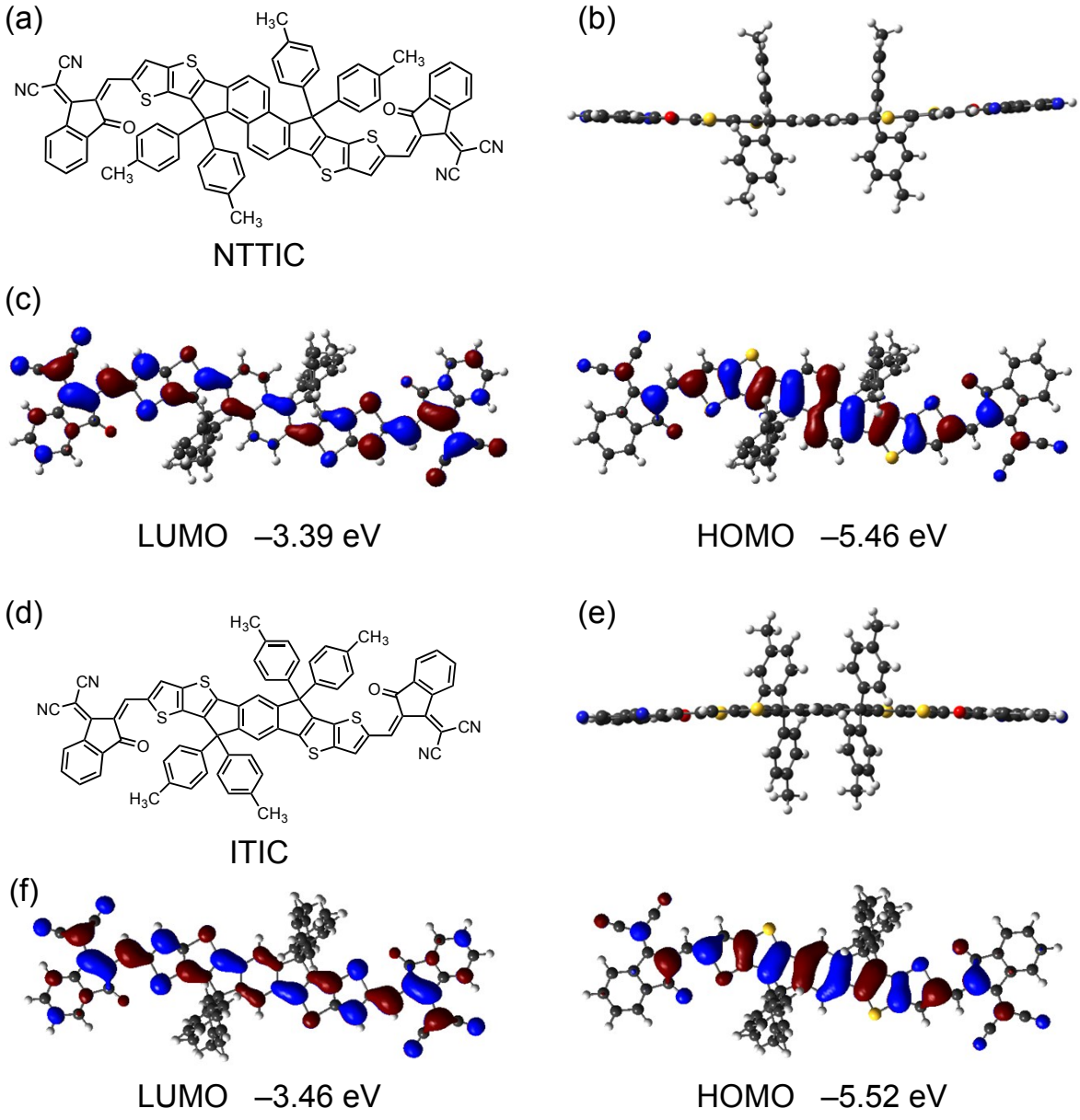


**Fig. S9** (a) Structure of NTTIC. Alkyl chains were simplified to methyl groups. (b) Optimized structure (side view) and (c) contour plots of frontier molecular orbitals simulated by the DFT calculations using B3LYP/6-31G(d) model for the simplified NTTIC in chloroform. The energy levels are also shown. (d) Structure of ITIC. Alkyl chains were simplified to methyl groups. (e) Optimized structure (side view) and (f) contour plots of frontier molecular orbitals for the simplified ITIC in chloroform. The energy levels are also shown.

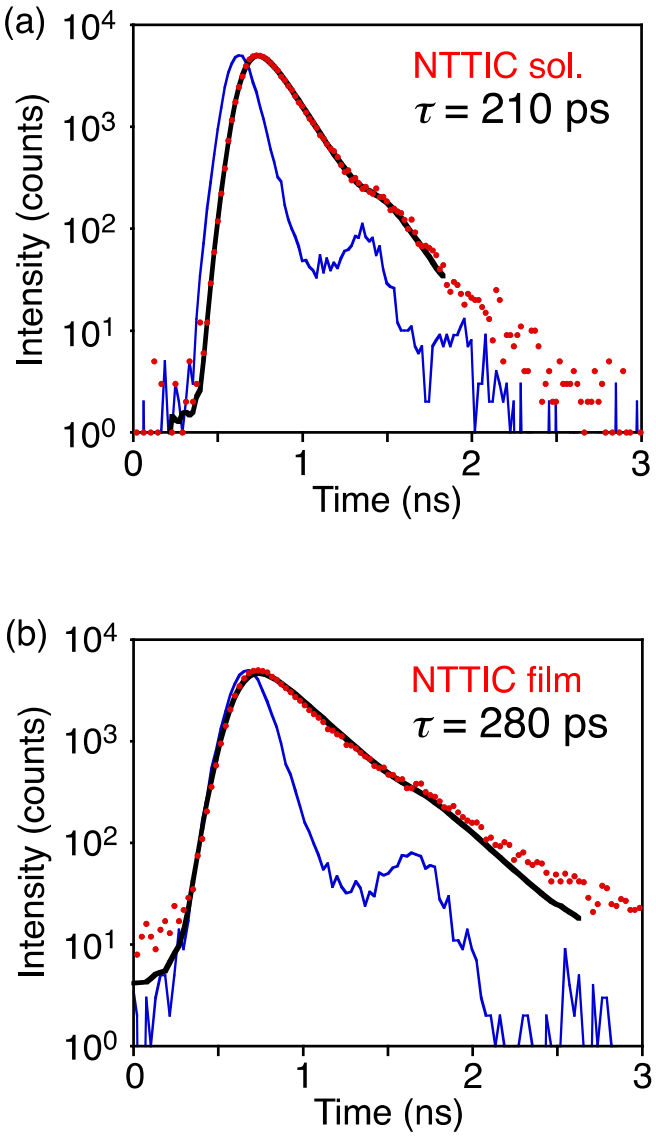


**Fig. S10** Nanosecond fluorescence decay (red), decay fitting (black line), and instrumental response function (blue line) of NTTIC (a) in chloroform and (c) film measured by the TCSPC technique. The excitation wavelength was 636 nm. The emission was detected at the maximum wavelength. The fluorescence lifetimes ($\tau$) are also shown in the figures.

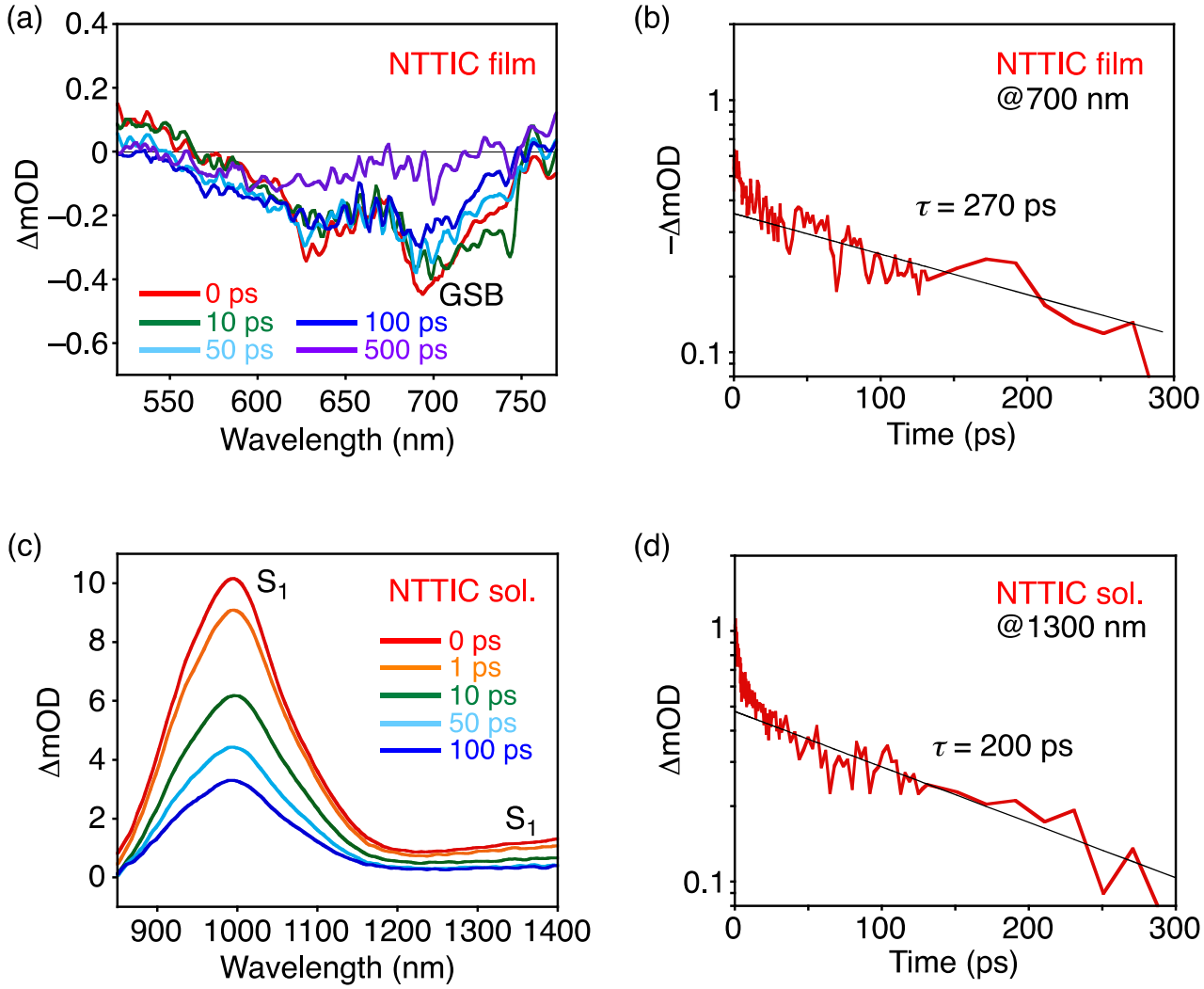


**Fig. S11** (a) Transient absorption spectra of the NTTIC film measured at 0–500 ps. The excitation wavelength and intensity were 620 nm and 0.36 μJ $cm^{-2}$, respectively. (b) Transient absorption profile of GSB of NTTIC film at 700 nm (red) and its fitting (black) in time range of 0–300 ps. The lifetime of GSB, i.e., the $S_1$ state, was calculated to be 270 ps. (c) Transient absorption spectrum of NTTIC solution in chloroform measured at 0–100 ps. The excitation wavelength and intensity were 700 nm and 26.9 μJ $cm^{-2}$, respectively. (d) Transient absorption profile of the $S_1$ state of NTTIC film at 1300 nm (red) and its fitting (black) in time range of 0–300 ps. The lifetime of the $S_1$ state was calculated to be 200 ps.

To avoid the singlet–singlet annihilation (SSA), the NTTIC film was excited at 620 nm, where the absorption intensity is lower than at 700 nm (Fig. S7a), with the low excitation intensity of 0.36 μJ $cm^{-2}$ in (a) and (b). In addition, the relatively clear GSB signal at 700 nm was monitored in (b).

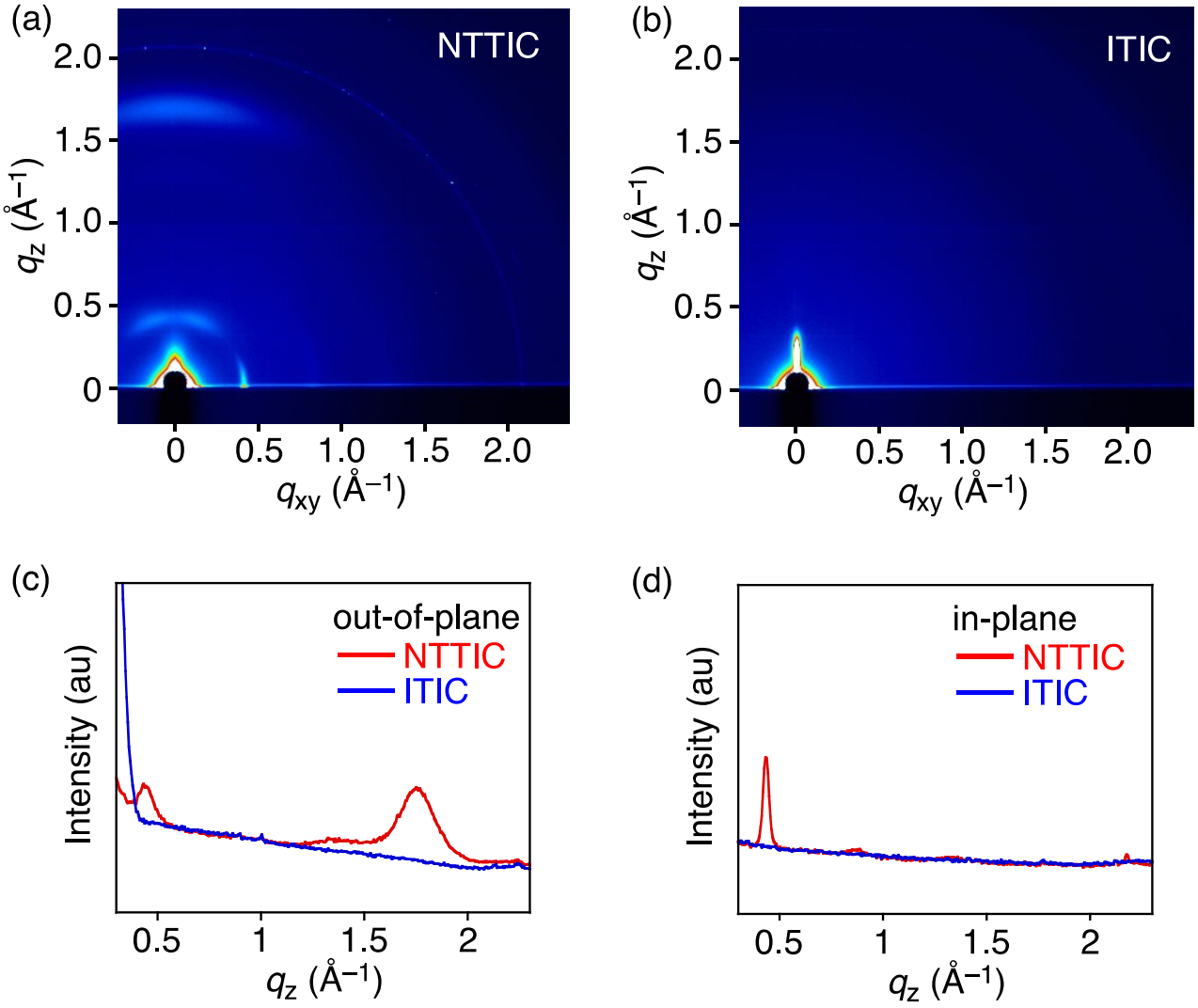


**Fig. S12** Two dimensional GIWAXS plots of (a) NTTIC and (b) ITIC neat films on ITO/ZnO substrates. (c) Out-of-plane and (d) in-plane GIWAXS profiles for NTTIC and ITIC neat films.

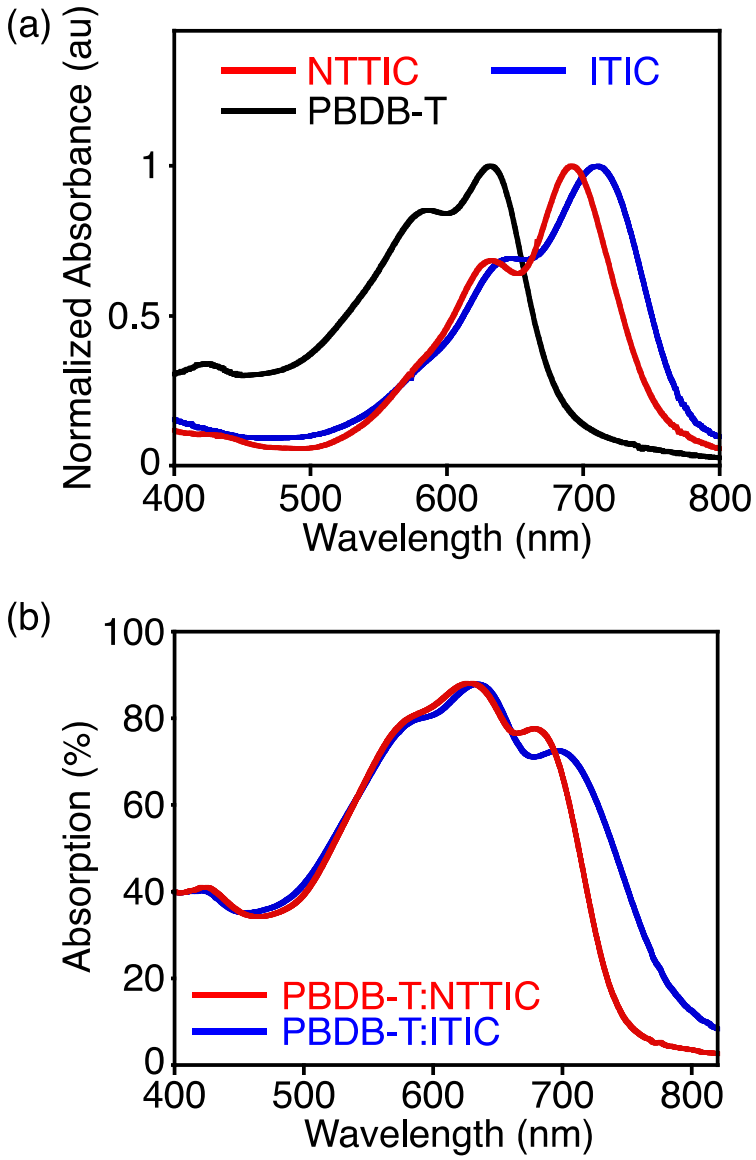


**Fig. S13** (a) Normalized UV–vis–NIR absorption spectra of NTTIC, ITIC, and PBDB-T neat films. (b) UV–vis–NIR absorption spectra of PBDB-T:NTTIC and PBDB-T:ITIC on ITO/ZnO substrates. Note here that the total absorption of the ITO/ZnO/PBDB-T:NFA/$MoO_3$/Ag devices is higher than the value in (b) because of the reflection from the Ag electrode.

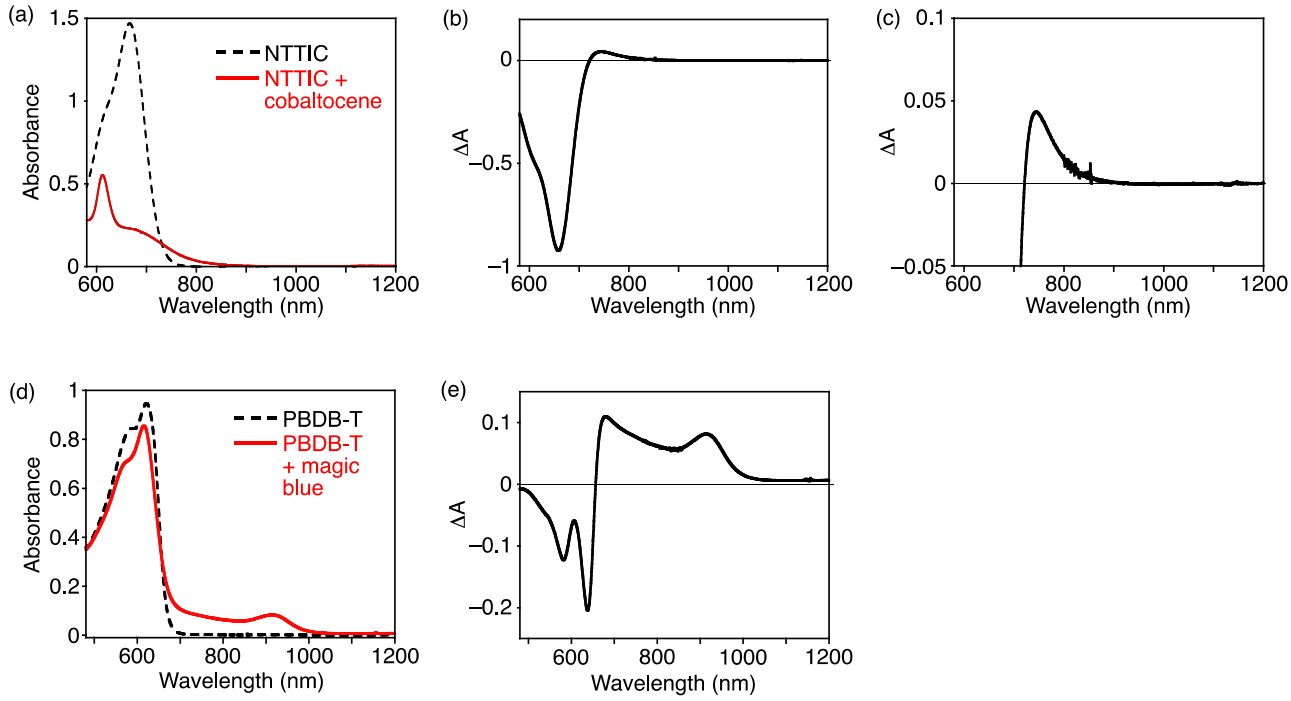


**Fig. S14** (a) Vis–NIR absorption spectra of NTTIC ($1.0 \times 10^{-5}$ M) (black dotted line) and NTTIC ($1.0 \times 10^{-5}$ M) with cobaltocene ($1.0 \times 10^{-5}$ M) as a reductant (red solid line) in benzonitrile. (b,c) Differential spectrum ((red solid line) – (black dotted line) in (a)) corresponding to the absorption of NTTIC anion. (d) Vis–NIR absorption spectra of PBDB-T ($1.4 \times 10^{-8}$ M by repeating unit) (black dotted line) and PBDB-T ($1.4 \times 10^{-8}$ M by repeating unit) with magic blue ($3.2 \times 10^{-9}$ M) as an oxidant (red solid line) in $CHCl_3$. (e) Differential spectrum ((red solid line) – (black dotted line) in (d)) corresponding to the absorption of PBDB-T hole polaron.

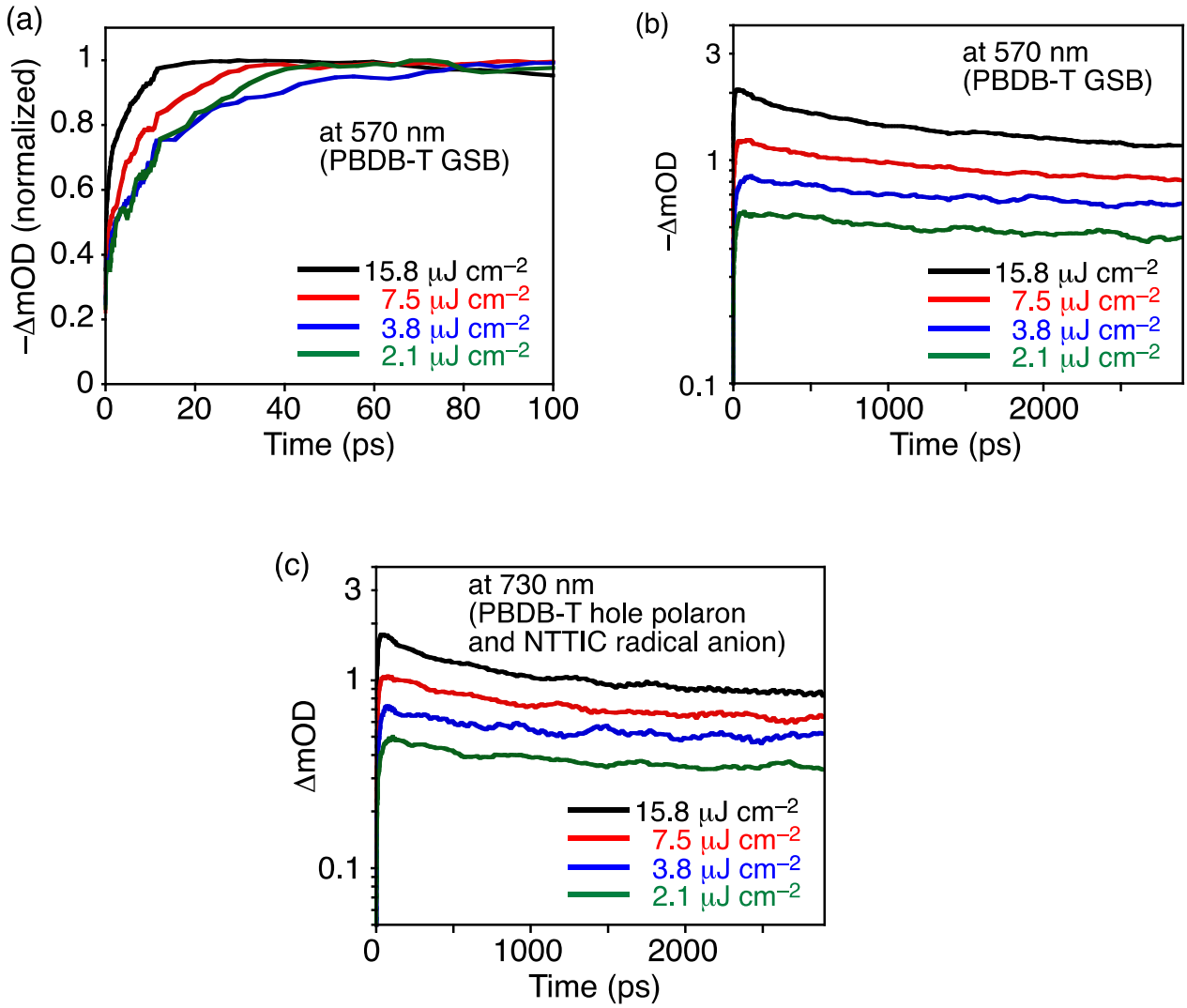


**Fig. S15** (a,b) Transient absorption profile of GSB of PBDB-T in PBDB-T:NTTIC blend film at 570 nm in time ranges of (a) 0–100 ps and (b) 0–2900 ps. (c) Transient absorption profile of PBDB-T hole polaron and NTTIC radical anion at 730 nm. The excitation wavelength was 700 nm and the excitation intensity ranged from 2.1 to 15.8 μJ $cm^{-2}$.

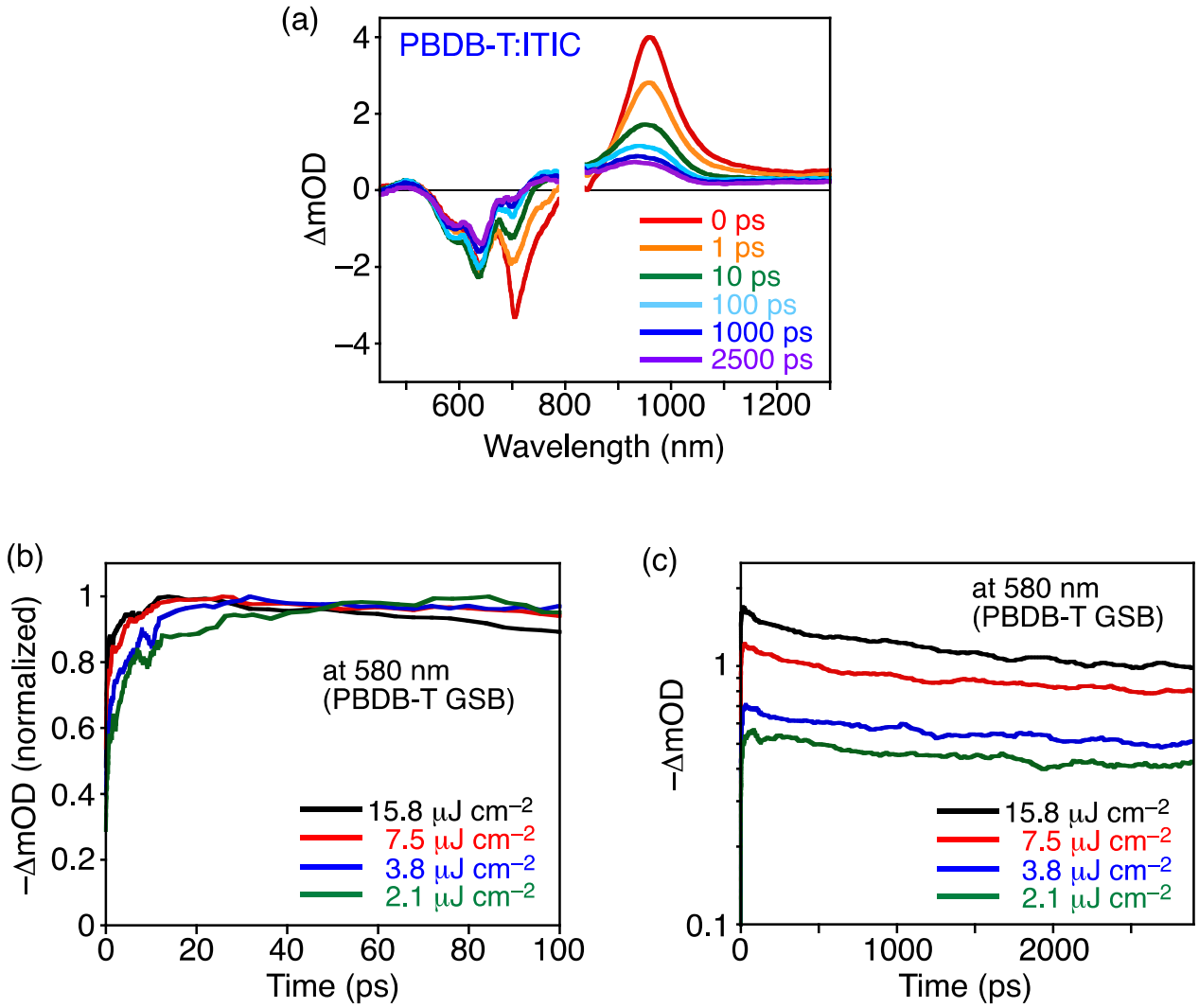


**Fig. S16** (a) Transient absorption spectra of the PBDB-T:ITIC blend film measured at 0–2500 ps. The excitation wavelength and intensity were 700 nm and 7.5 μJ $cm^{-2}$, respectively. (b,c) Transient absorption profile of GSB of PBDB-T in the PBDB-T:ITIC blend film at 580 nm in time ranges of (b) 0–100 ps and (c) 0–2900 ps. The excitation wavelength was 700 nm and the excitation intensity ranged from 2.1 to 15.8 μJ $cm^{-2}$.

Signal assignments and discussion on the decay dynamics of $S_1$ of ITIC and charge-separated states in PBDB-T:ITIC with various excitation intensities were already described in the previous report.[S9]

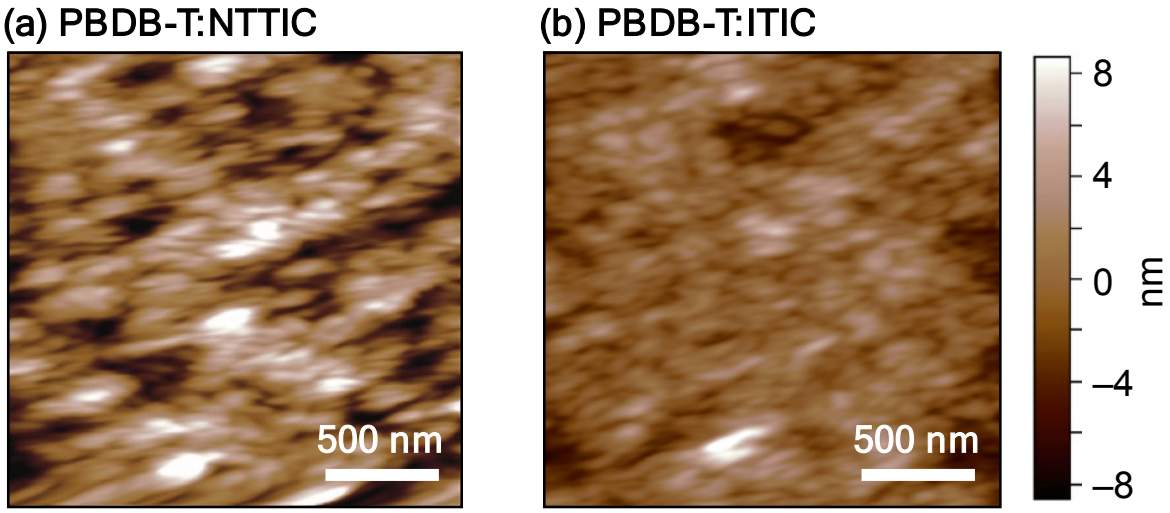


**Fig. S17** AFM images of (a) PBDB-T:NTTIC and (b) PBDB-T:ITIC on ITO/ZnO substrates. The color scale represents the height topography, with bright and dark representing the highest and lowest features, respectively. The root-mean-square (rms) surface roughness of PBDB-T:NTTIC (3.7 nm) is larger than that of PBDB-T:ITIC (1.1 nm).

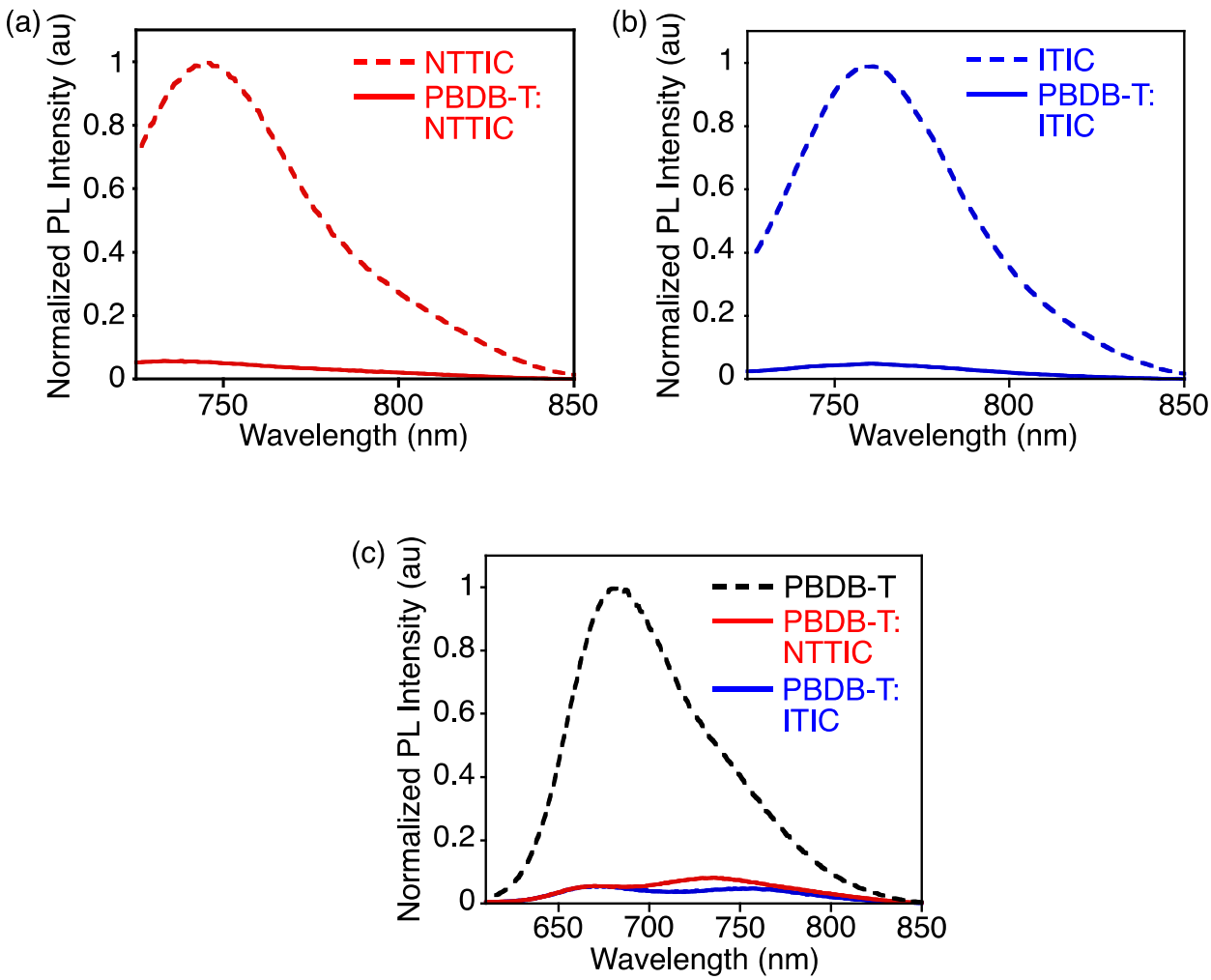


**Fig. S18** PL spectra of (a) NTTIC single component film (red dotted) and PBDB-T:NTTIC (red solid) and (b) ITIC single component film (blue dotted) and PBDB-T:ITIC (blue solid). The samples were excited at 710 nm, where the NFAs were preferentially excited. The emission intensities are normalized by that of the NFA single component film considering the difference in the absorbances of the PBDB-T:NFA films at the excitation wavelength. (c) PL spectra of PBDB-T single component film (black dotted) and blend films of PBDB-T with NTTIC (red solid) and ITIC (blue solid). The excitation wavelength was 520 nm where PBDB-T was preferentially excited. The emission intensities are normalized by that of the PBDB-T single component film considering the difference in the absorbances of the PBDB-T:NFA films at the excitation wavelength.

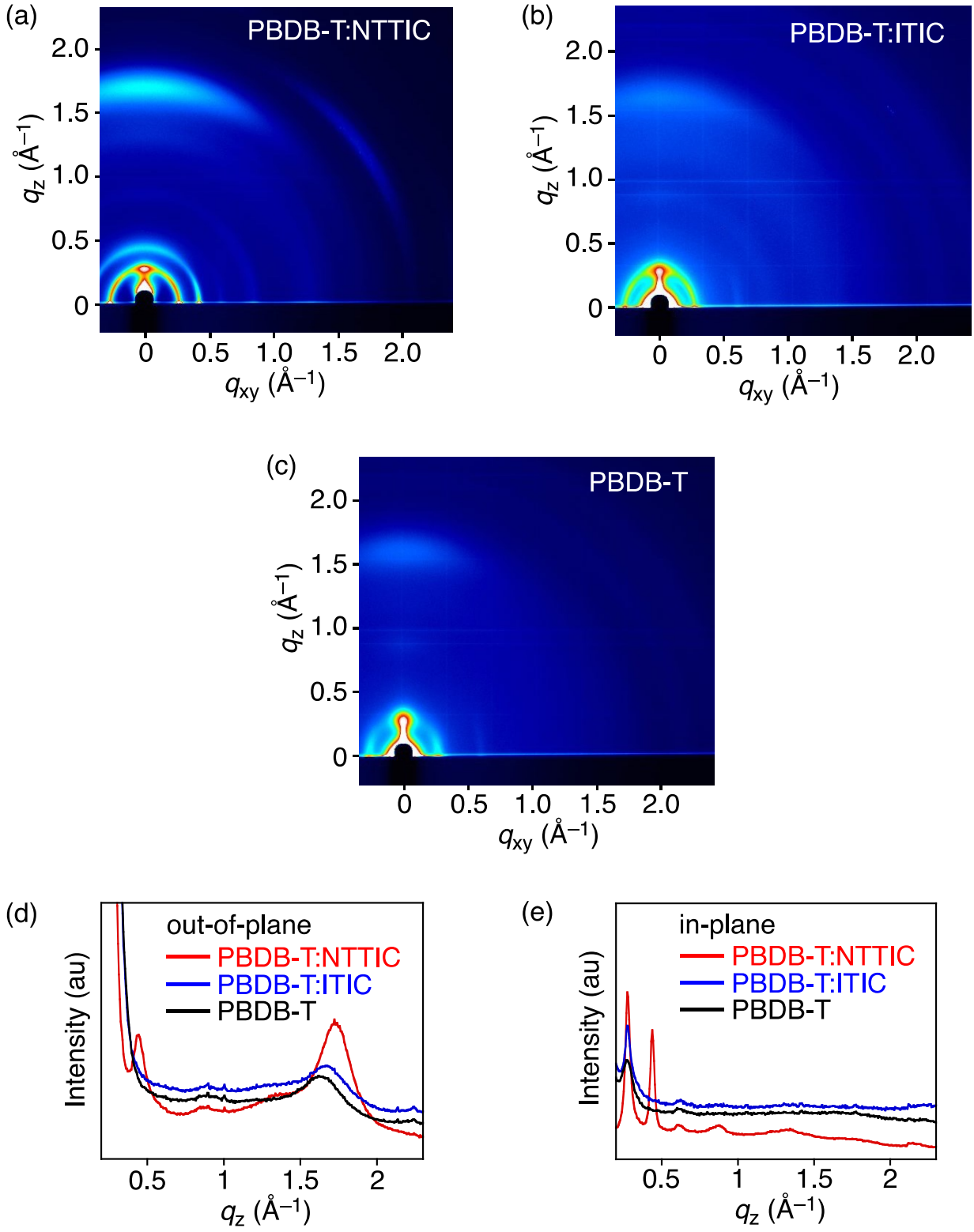


**Fig. S19** Two dimensional GIWAXS plots of (a) PBDB-T:NTTIC, (b) PBDB-T:ITIC, and (c) PBDB-T on ITO/ZnO substrates. (d) Out-of-plane and (e) in-plane GIWAXS profiles of PBDB-T:NTTIC, PBDB-T:ITIC, and PBDB-T.

## References


(S1) M. J. Frisch, G. W. Trucks, H. B. Schlegel, G. E. Scuseria, M. A. Robb, J. R. Cheeseman, G. Scalmani, V. Barone, B. Mennucci, G. A. Petersson, H. Nakatsuji, M. Caricato, X. Li, H. P. Hratchian, A. F. Izmaylov, J. Bloino, G. Zheng, J. L. Sonnenberg, M. Hada, M. Ehara, K. Toyota, R. Fukuda, J. Hasegawa, M. Ishida, T. Nakajima, Y. Honda, O. Kitao, H. Nakai, T. Vreven, J. A. Montgomery, Jr., J. E. Peralta, F. Ogliaro, M. Bearpark, J. J. Heyd, E. Brothers, K. N. Kudin, V. N. Staroverov, T. Keith, R. Kobayashi, J. Normand, K. Raghavachari, A. Rendell, J. C. Burant, S. S. Iyengar, J. Tomasi, M. Cossi, N. Rega, J. M. Millam, M. Klene, J. E. Knox, J. B. Cross, V. Bakken, C. Adamo, J. Jaramillo, R. Gomperts, R. E. Stratmann, O. Yazyev, A. J. Austin, R. Cammi, C. Pomelli, J. W. Ochterski, R. L. Martin, K. Morokuma, V. G. Zakrzewski, G. A. Voth, P. Salvador, J. J. Dannenberg, S. Dapprich, A. D. Daniels, O. Farkas, J. B. Foresman, J. V. Ortiz, J. Cioslowski and D. J. Fox, *Gaussian 09, revision D.01*, Gaussian, Inc., Wallingford, CT, 2013.

(S2) D. He, L. Qian and L. Ding, *Polym. Chem.*, 2016, **7**, 2329.

(S3) M. Hori, J. D. Guo, T. Yanagi, K. Nogi, T. Sasamori and H. Yorimitsu, *Angew. Chem. Int. Ed.*, 2018, **57**, 4663.

(S4) Y. Cui, H. Ren, J. Yu, Z. Wang and G. Qian, *Dyes Pigm.*, 2009, **81**, 53.

(S5) J. M. Tobin, J. Liu, H. Hayes, M. Demleitner, D. Ellis, V. Arrighi, Z. Xu and F. Vilela, *Polym. Chem.*, 2016, **7**, 6662.

(S6) B. Kan, J. Zhang, F. Liu, X. Wan, C. Li, X. Ke, Y. Wang, H. Feng, Y. Zhang, G. Long, R. H. Friend, A.A. Bakulin and Y. Chen, *Adv. Mater.*, 2018, **30**, 1704904.

(S7) O. M. Awartani, B. Gautam, W. Zhao, R. Younts, J. Hou, K. Gundogdu and H. Ade, *J. Mater. Chem. A*, 2018, **6**, 12484.

(S8) T. R. Hopper, D. Qian, L. Yang, X. Wang, K. Zhou, R. Kumar, W. Ma, C. He, J. Hou, F. Gao and A. A. Bakulin, *Chem. Mater.*, 2019, **31**, 6860.

(S9) T. Umeyama, K. Igarashi, D. Sasada, Y. Tamai, K. Ishida, T. Koganezawa, S. Ohtani, K. Tanaka, H. Ohkita and H. Imahori, *Chem. Sci.*, 2020, **11**, 3250.